LETTER

doi:10.1038/nature14319

Disruption of DNA-methylation-dependent long gene repression in Rett syndrome

Harrison W. Gabel[1]*, Benyam Kinde[1]*, Hume Stroud[1], Caitlin S. Gilbert[1], David A. Harmin[1], Nathaniel R. Kastan[1], Martin Hemberg[2]†, Daniel H. Ebert[1] & Michael E. Greenberg[1]

Disruption of the *MECP2* gene leads to Rett syndrome (RTT), a severe neurological disorder with features of autism[1]. *MECP2* encodes a methyl-DNA-binding protein[2] that has been proposed to function as a transcriptional repressor, but despite numerous mouse studies examining neuronal gene expression in *Mecp2* mutants, no clear model has emerged for how MeCP2 protein regulates transcription[3–9]. Here we identify a genome-wide length-dependent increase in gene expression in MeCP2 mutant mouse models and human RTT brains. We present evidence that MeCP2 represses gene expression by binding to methylated CA sites within long genes, and that in neurons lacking MeCP2, decreasing the expression of long genes attenuates RTT-associated cellular deficits. In addition, we find that long genes as a population are enriched for neuronal functions and selectively expressed in the brain. These findings suggest that mutations in MeCP2 may cause neurological dysfunction by specifically disrupting long gene expression in the brain.

To identify common features of genes whose expression is misregulated in RTT, we surveyed gene expression data sets from studies of *Mecp2* mutant mice, asking if genes that are misregulated when MeCP2 function is disrupted have anything in common with respect to histone modifications, mRNA expression, sequence composition or gene length. No common features were identified for genes that are downregulated when MeCP2 function is disrupted; however, we found that genes that are upregulated in the *Mecp2* knockout brains are significantly longer than the genome-wide average (Fig. 1a). The extreme length of the genes upregulated in MeCP2 knockout brains is apparent in multiple studies performed by different laboratories[5–9] (Supplementary Table 1). The misexpression of long genes is a specific feature of the RTT brain, as gene sets identified as misregulated in 16 different mouse models of neurological dysfunction and disease did not display similarly long length (Extended Data Fig. 1).

To determine whether the extent of gene misregulation in *Mecp2* mutant mice is directly correlated with gene length, we interrogated published microarray data sets of gene expression and plotted mRNA fold-change (MeCP2 knockout compared to wild type) versus gene length[10]. We found widespread length-dependent misregulation of gene expression in MeCP2 knockout brains, with the longest genes in the genome displaying the highest level of upregulation relative to shorter genes, which show a reduction or no change in gene expression (Fig. 1b, c and Extended Data Fig. 1). Consistent with previous studies, the magnitude of the length-dependent gene misregulation in the absence of MeCP2 is small, but widespread (affecting genes across the continuum of gene lengths) and reproducibly detected (Fig. 1b and Extended Data Fig. 1). Importantly, length-dependent gene misregulation in the MeCP2 knockout is not an artefact of the method of gene expression analysis used, as this effect was detected using a variety of methodologies including microarrays, total RNA-seq, quantitative PCR, and non-amplification-based nCounter analysis (Fig. 1b, c and Extended Data Fig. 1 and Supplementary Discussion). Furthermore, these observations are corroborated by the recent finding[11] that long genes are upregulated in specific neuronal cell types when MeCP2 function is disrupted.

Additional copies of *MECP2* cause neurological impairment in humans (MeCP2-duplication syndrome) and in transgenic mice[12,13]. We find that overexpression of MeCP2 in mice leads to the downregulation of long genes in the brain[5–7] (Fig. 1b and Extended Data Fig. 1). This further suggests that MeCP2 directly represses transcription in a length-dependent manner.

We next investigated if the length-dependent changes in gene expression correlate with the onset and severity of RTT pathology. We found that misregulation of long gene expression in the brain of MeCP2 knockout mice is more striking at nine weeks of age than at four weeks of age[8], thus correlating with disease progression (Extended Data Fig. 2). In addition, when comparing two disease-causing MeCP2 mutations (MeCP2(R270X) and MeCP2(G273X)) that differ in the rate and severity with which they cause disease, we find that the magnitude of length-dependent gene misregulation correlates with the severity of RTT phenotypes[8] (Extended Data Fig. 2 and Supplementary Discussion). Furthermore, we find by microarray, nCounter and qRT–PCR analysis that a subtle missense mutation of MeCP2 (Arg 306 to Cys, R306C) that causes RTT in humans and disrupts the interaction of MeCP2 with the NCoR co-repressor complex[14] leads to length-dependent gene upregulation in the mouse brain (Extended Data Fig. 1). Finally, we detect length-dependent gene upregulation in cultured human neurons derived from embryonic stem cells lacking MECP2 (ref. 15) and the cortex of humans with RTT[16] (Fig. 1d and Extended Data Fig. 2 and Supplementary Discussion). The close correlation between the occurrence of length-dependent gene misregulation and RTT-associated phenotypes across mice and humans suggests that this misregulation contributes to RTT pathology.

To characterize the mechanism by which MeCP2 tempers the expression of long genes, we asked if the binding of MeCP2 to methylated DNA is important for this process. MeCP2 was identified based on its high affinity for methylated cytosine in the context of a CpG dinucleotide (mCG)[17]. In addition to binding mCG, MeCP2 has been suggested to bind two additional forms of methylated DNA that are enriched in the brain, hydroxymethylcytosine (hmC)[18] and methylated cytosine followed by a nucleotide other than guanine (mCH, where H = A or T or C)[19]. Notably, the frequency of hmCG and mCH in the neuronal genome increases significantly during the same postnatal period in which the level of MeCP2 protein markedly increases[20–24]. This suggests that as neurons mature, MeCP2 could function by binding to hmCG and/or mCH marks. Using a DNA electrophoretic mobility shift assay (EMSA) we assessed the binding of MeCP2 to various forms of methylated DNA. Consistent with previous studies, we find that MeCP2 shows high affinity for DNA containing mCG but not hmCG, suggesting that MeCP2 may not bind preferentially to hmCG in neurons (Fig. 2a,

[1]Department of Neurobiology, Harvard Medical School, Boston, Massachusetts 02115, USA. [2]Department of Ophthalmology, Children's Hospital Boston, Center for Brain Science and Swartz Center for Theoretical Neuroscience, Harvard University, 300 Longwood Avenue, Boston, Massachusetts 02115, USA. †Present address: Computational Genomics Programme, Wellcome Trust Sanger Institute, Wellcome Trust Genome Campus, Hinxton, Cambridge CB10 1SA, UK.
*These authors contributed equally to this work.

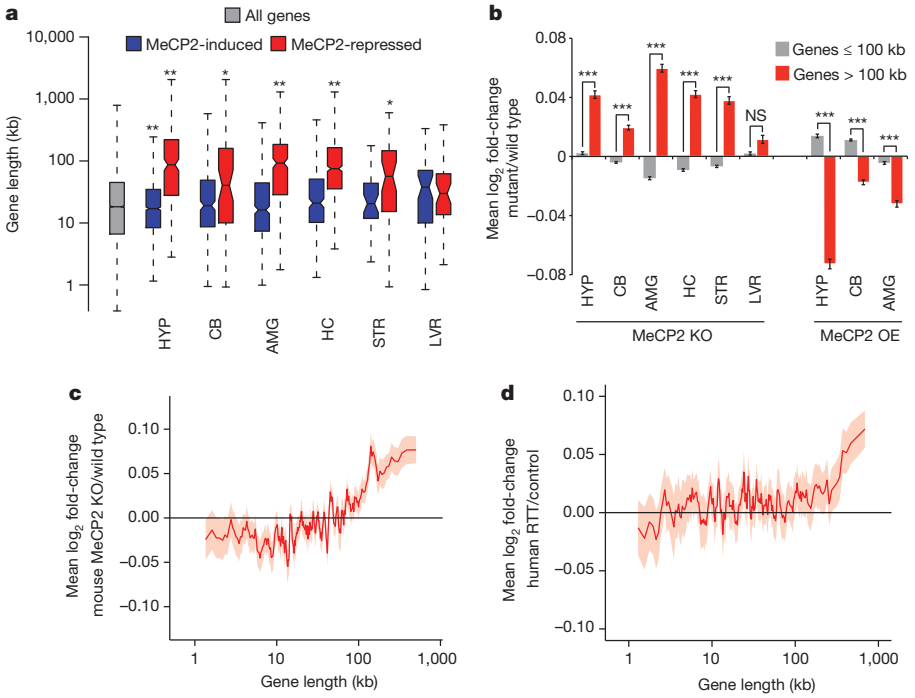

Figure 1 | Length-dependent gene misregulation in *Mecp2* mutant mice and human RTT brain. **a**, Boxplots (showing the median (line), second to third quartiles (box), 1.5× the interquartile range (whiskers), and 1.58× the interquartile range/($\sqrt{}$ number of genes)) of gene lengths (RefSeq transcription start site to termination site) for genes detected as misregulated in independent studies of *Mecp2* mutant mice. HYP, hypothalamus[5]; CB, cerebellum[6]; AMG, amygdala[7]; HC, hippocampus[8]; STR, striatum[9]; LVR, liver[9]. MeCP2-induced (blue), genes downregulated in MeCP2 knockout (MeCP2 KO) and upregulated in MeCP2 overexpression (MeCP2 OE) mice. MeCP2-repressed (red), genes upregulated in MeCP2 KO and downregulated in MeCP2 OE (see Methods). **b**, Mean expression changes across brain regions and liver of *Mecp2* mutant mice for genes ≤ 100 kb (grey) and >100 kb (red) (see Methods and Supplementary Table 1 for sample sizes and other details). **c**, **d**, Genome-wide changes in gene expression assessed by RNA-seq analysis of mouse cortical tissue from MeCP2 KO ($n = 3$) compared to wild type ($n = 3$) (**c**) or microarray analysis of human RTT brain samples ($n = 3$) compared to age-matched controls ($n = 3$)[16] (**d**). In **c**, **d** lines represent mean fold-change in expression for genes binned according to gene length (200 gene bins, 40 gene step; see Methods); the ribbon is the s.e.m. of each bin. $^{*}P < 0.05$; $^{**}P < 0.01$; $^{***}P < 1 \times 10^{-10}$, NS, not significant $P \geq 0.05$; one-sample (**a**) or two sample (**b**) *t*-test, Bonferroni correction. Error bars represent s.e.m.

Extended Data Fig. 3 and Supplementary Discussion). By contrast, MeCP2 binds to mCA, hmCA and mCG with relatively high affinity, but binds to mCC and mCT with low affinity similar to that of unmethylated DNA. This selective, tight binding of MeCP2 to mCG, mCA and hmCA suggests that MeCP2 may regulate long gene expression in the brain by binding to these sites. We note that thin-layer chromatography and Tet-assisted bisulfite sequencing (TAB-seq) analysis suggest that hmCA is very rare in the brain[21,24]. Therefore, in our subsequent investigation of MeCP2 binding to CA sequences *in vivo* we focused our analysis on mCA. However, at genomic sites where CA sequences are hydroxymethylated, MeCP2 might also be predicted to bind and regulate gene expression (see Supplementary Discussion).

To examine whether MeCP2 binds mCA in the brain, we performed chromatin immunoprecipitation sequencing analysis (ChIP-seq) of MeCP2, comparing the MeCP2 binding profile across the genome to base-pair resolution DNA methylation data (see Methods)[24]. As previously reported[20,25], we find that MeCP2 binds broadly across the genome. Nevertheless, within the context of this broad binding, we detect a relative enrichment of MeCP2 at gene bodies that have a high level of mCA (level = (h)mCN/CN within the gene, see Methods), and a depletion of MeCP2 binding at gene bodies where the level of hmCG is high (Extended Data Fig. 4). Notably, long genes (> 100 kb) display a strong relationship between mCA levels and MeCP2 ChIP-seq read density (Fig. 2b and Extended Data Fig. 4). Higher-resolution analysis of MeCP2 ChIP and mCA levels in the frontal cortex revealed increased mCA under sites of local MeCP2 enrichment in the genome, supporting the conclusion that MeCP2 binds to mCA *in vivo* (Extended Data Fig. 4). We note that genes containing the highest level of hmCA are also enriched for the MeCP2 ChIP signal (Extended Data Fig. 4). Therefore, if owing to limitations of the methods of analysis the amount of hmCA within gene bodies is being underestimated, some of the effects of MeCP2 deletion that are being attributed to MeCP2 binding to mCA might be due to MeCP2 binding to hmCA (see Supplementary Discussion).

To investigate if length-dependent gene repression by MeCP2 requires binding to mCA, we assessed whether there is a correlation between the degree of misregulation of gene expression upon the disruption of MeCP2 function and the levels of DNA methylation within the transcribed regions of genes (see Supplementary Discussion). We noted a trend whereby genes containing high levels of mCA, but not mCG or hmCG, are upregulated in the MeCP2 knockout (Extended Data Figs 5 and 6). We reasoned that if mCA within genes is required for length-dependent repression by MeCP2, long genes containing low levels of mCA should be largely unaffected in the MeCP2 knockout mice. Consistent with this prediction, little to no length-dependent upregulation of gene expression is observed in MeCP2 knockout brain for genes containing low levels of mCA, while long genes with a high density of mCA are significantly upregulated in MeCP2 knockout brains. In addition, we found that the shortest genes in the genome are not upregulated when MeCP2 function is disrupted, even when the average level of mCA within their gene body is relatively high (Fig. 2c and Extended Data Fig. 6). The requirement for the presence of mCA within long genes for the gene to be repressed by MeCP2 is reproducible, as it is detected across three MeCP2 knockout brain regions, in gene expression data from MeCP2(R306C) and MeCP2 overexpressing mice, and in human RTT brain (Fig. 2d and Extended Data Fig. 6). Notably, when we plotted the level of mCA versus gene length, we found that the density of mCA is higher on average in longer genes compared to shorter genes (Extended Data Figs 5 and 6). The enrichment of mCA

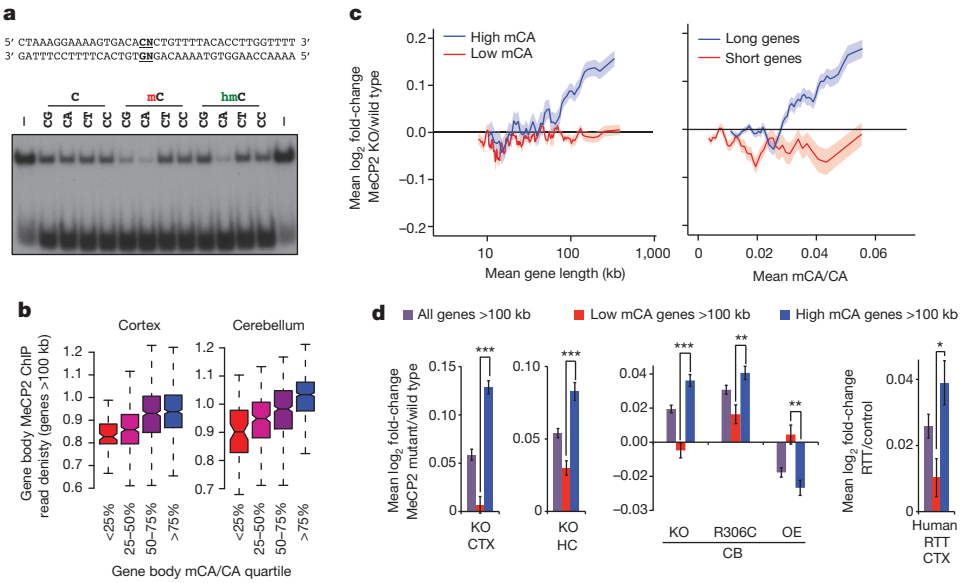

Figure 2 | MeCP2 represses long genes containing high levels of mCA. **a**, EMSA analysis of the MeCP2 methyl-binding domain (amino acids 78–162) binding to ^{32}P-end-labelled mCA-containing DNA probe incubated with 100-fold excess of unlabelled competitor oligonucleotides containing unmodified, methylated, or hydroxymethylated cytosines at the dinucleotides indicated in bold; no competitor indicated by − symbol (see Methods and Extended Data Fig. 3). **b,** Boxplots of MeCP2 ChIP-seq read density within genes > 100 kb plotted by quartile of mCA/CA in the cortex and cerebellum. **c,** Mean fold-change in gene expression binned according to gene length in MeCP2 knockout cortical tissue for genes with high (mCA/CA >0.034, top 25%) and low (mCA/CA <0.031, bottom 66%) mCA levels (left), or binned according to gene-body mCA/CA levels for long (> 62 kb, top 25%) and short (< 16.8 kb, shortest 25%) genes (right). Lines represent mean fold-change in expression for each bin (200 gene bins, 40 gene step), and the ribbon is s.e.m. of each bin. $n = 3$ per genotype. **d**, Bar plots of the mean fold-change in expression for all genes > 100 kb compared to subsets of genes > 100 kb containing low mCA (bottom 50% mCA/CA) or high mCA (top 25% mCA/CA) within their gene body. Values shown for mice with the indicated *Mecp2* genotypes (left) and human RTT brain (right). CTX, Cortex; HC, Hippocampus; CB, cerebellum; KO, MeCP2 knockout; OE, MeCP2 overexpression; R306C, MeCP2 arginine 306 to cysteine missense mutation; $***P < 1 \times 10^{-10}$; $**P < 1 \times 10^{-3}$; $*P < 0.01$; two-tailed *t*-test, Bonferroni correction. Error bars represent s.e.m. See Supplementary Table 1 for sample size and other details.

within long genes may explain why most of these genes are repressed by MeCP2 and upregulated in the MeCP2 knockout.

To test further whether MeCP2 tempers long gene transcription by binding to mCA within genes, we asked if elimination of mCA in the brain has an effect on gene expression that is similar to that observed in the MeCP2 knockout. Recent evidence suggests that Dnmt3a is the enzyme that catalyses the deposition of mCA in maturing neurons[19,24]. We therefore conditionally disrupted the *Dnmt3a* gene[26] in the brain to block the accumulation of mCA (*Nestin-Cre*; Dnmt3a$^{fl/fl}$ mice, designated Dnmt3a cKO, Extended Data Fig. 7 and Supplementary Discussion). Bisulfite sequencing of cerebellum DNA indicated that methylation of DNA at CA, but not CG, is eliminated from the genome in the Dnmt3a conditional knockout (Fig. 3a). Microarray analysis of cerebella from Dnmt3a conditional knockout mice revealed a length- and mCA-dependent upregulation of gene expression that is similar to the gene misregulation detected in MeCP2 knockout mice (Fig. 3b and Extended Data Fig. 8). While the deletion of Dnmt3a also leads to a decrease in methylation at CT and CC, given that MeCP2 selectively binds to mCA *in vitro*, we conclude that reduction of mCA within gene bodies in the Dnmt3a conditional knockout probably disrupts length-dependent gene repression by MeCP2. Taken together, these findings support a model in which Dnmt3a catalyses the methylation of CA in the neuronal genome. MeCP2 then binds to these sites within the transcribed regions of genes to restrain transcription in a length-dependent manner.

To characterize how the misregulation of long gene expression contributes to RTT pathology, we identified a representative set of genes that is consistently misregulated in multiple gene expression data sets when MeCP2 function is perturbed. Combined analysis of microarray studies across multiple brain regions identified 466 MeCP2-repressed genes whose expression is consistently upregulated in MeCP2 knockout

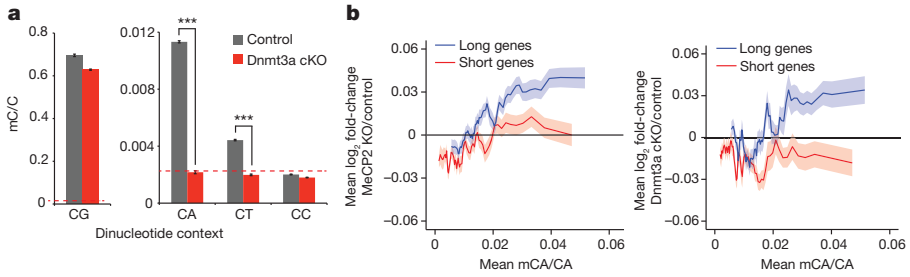

Figure 3 | Disruption of Dnmt3a in the brain leads to length-dependent upregulation of genes containing high levels of mCA. **a**, Summary of genome-wide bisulfite-sequencing analysis of mCN (where N = G, A, T or C) in control and Dnmt3a cKO cerebella ($n = 2$ per genotype). Dashed line represents mean background non-conversion rate of the bisulfite-seq assay (see Methods). **b**, Mean fold-change in gene expression versus gene-body mCA for MeCP2 KO (left) or Dnmt3a cKO (right) cerebella. Long (top 25%, > 60 kb) and short (bottom 25%, < 14.9 kb) genes were binned according to gene-body mCA/CA levels. Lines represent mean fold-change in expression for each bin (200 gene bins, 40 gene step), and the ribbon is s.e.m. of genes within each bin. $***P < 0.005$; two-tailed *t*-test, Bonferroni correction. Error bars represent s.e.m. $n = 5$ per genotype for for MeCP2 KO, $n = 3$ per genotype for Dnmt3a cKO.

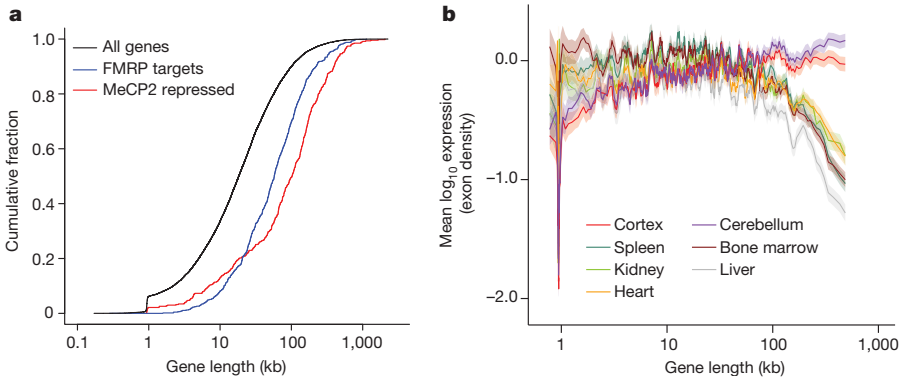

Figure 4 | Analysis of long gene expression and regulation in the brain. **a**, Cumulative distribution function of gene lengths for all genes in the genome (black), MeCP2-repressed genes (red), and genes encoding putative FMRP target mRNAs[29] (blue); $P < 1 \times 10^{-15}$ for each gene set versus all genes, two-sample Kolmogorov–Smirnov test. **b**, Mean expression of genes binned according to length in mouse for neural and non-neural tissues. Line indicates mean expression for genes within each bin (200 gene bins, 40 gene step); the ribbon represents the s.e.m. of each bin.

mice and downregulated in MeCP2 overexpressing mice (Supplementary Discussion and Supplementary Table 3). Consistent with the conclusion that MeCP2-repressed genes are targets of gene-length- and mCA-dependent repression, these genes are exceptionally long and are enriched for mCA (Fig. 4a and Extended Data Fig. 8). Disruption of the expression of this gene set is specific to RTT, as these genes were not misregulated in data sets obtained from six other mouse models of neurological dysfunction (Extended Data Fig. 8).

We examined the functional annotations of the 466 MeCP2-repressed genes to gain insight into how their disruption might contribute to RTT pathology. Many of these MeCP2-repressed genes encode proteins that modulate neuronal physiology (for example, calcium/calmodulin-dependent kinase *Camk2d* and the voltage-gated potassium channel *Kcnh7*). In addition, multiple genes involved in axon guidance and synapse formation were identified, including *Epha7*, *Sdk1* and *Cntn4* (Extended Data Fig. 8). Consistent with these observations, gene ontology analysis of MeCP2-repressed genes indicates that they are enriched for annotated neuronal functions (for example, post-synaptic density, axonogenesis, voltage-gated cation channel activity; Extended Data Table 1). These findings suggest that RTT results from a subtle, yet widespread overexpression of long genes that have specific functions in the nervous system.

We next considered why the misregulation of long genes as a population in RTT leads specifically to neuronal dysfunction. Many genes with neuronal function are very long[27,28], raising the possibility that long genes as a population might be enriched for functions in the nervous system relative to other tissues. If so, the high level of mCA and MeCP2 in neurons may have evolved to temper the expression of long genes specifically in the brain. Indeed, gene ontology analysis of all genes in the genome above 100 kb indicates that the longest genes in the genome are enriched for neuronal annotations (Extended Data Table 1). Moreover, by examining tissue-specific gene expression data sets, we find that long genes as a population are preferentially expressed in mouse and human brain relative to other tissues (Fig. 4b and Extended Data Fig. 9). We note that while long genes typically have brain-specific function and expression, brain-specific expression is not a prerequisite for regulation of long genes by MeCP2 in neurons: some long genes are ubiquitously expressed but selectively repressed by MeCP2 in the brain. (Extended Data Fig. 8 and Supplementary Discussion).

To explore if disruption of proteins that regulate long gene expression may broadly contribute to autism spectrum disorders (ASDs), we asked if a similar misregulation of gene expression occurs in a prominent ASD, fragile X syndrome (FXS). FXS is caused by inactivation of FMRP, a protein that represses mRNA translation in neurons[29]. Strikingly, we find that FMRP-target mRNAs and the genes that encode them are significantly longer than the genome average[29] (Fig. 4a, Extended Data Fig. 8 and Supplementary Discussion). Moreover, we detect significant overlap between MeCP2-repressed genes and genes encoding FMRP-target mRNAs (Extended Data Fig. 8). These results suggest that upregulation of long gene function, either through increased transcription (RTT) or mRNA translation (FXS), may represent a common cause of pathology in neurodevelopmental disorders.

A recent study demonstrated that pharmacological inhibition of topoisomerases leads to the broad downregulation of long genes in neurons[10], suggesting that topoisomerase inhibitors might reverse the upregulation of long gene expression observed in the absence of MeCP2. To test this, we knocked-down MeCP2 expression in cultured cortical neurons with RNA-mediated interference (RNAi) and treated these cells with the topoisomerase inhibitor topotecan. We found that MeCP2 knockdown leads to the upregulation of long genes and that exposure of MeCP2-deficient neurons to topotecan results in a dose-dependent reversal of long gene misregulation (Extended Data Fig. 9).

The disruption of MeCP2 function in both mouse and human neurons leads to an overall reduction in cell health that can be measured as a decrease in the level of ribosomal RNA and cell size[15,30]. Notably, we found that the concentration of topotecan that most effectively reverses overexpression of long genes (50 nM) partially reverses the decreased ribosomal RNA content observed in neurons lacking MeCP2 (Extended Data Fig. 9). This result suggests that the rebalancing of long gene expression improves cell health in MeCP2 knockdown neurons, leading to increased cellular rRNA content. Taken together, these data suggest that rebalancing long gene expression in neurons lacking MeCP2 may attenuate the cellular dysfunction observed in these cells.

Our finding that long genes are misregulated in RTT, and that this misregulation can be reversed by topotecan treatment complements a recent study[10] implicating topoisomerases in the regulation of long genes in the brain. Thus, our study provides additional evidence that disruption of long gene expression may be a general mechanism underlying ASDs, and suggests that developing methods to rebalance long gene expression may be a strategy to correct neural dysfunction in these disorders.

Online Content Methods, along with any additional Extended Data display items and Source Data, are available in the online version of the paper; references unique to these sections appear only in the online paper.

Received 24 July 2014; accepted 12 February 2015.
Published online 11 March 2015.

1. Chahrour, M. & Zoghbi, H. Y. The story of Rett syndrome: from clinic to neurobiology. *Neuron* **56,** 422–437 (2007).
2. Guy, J., Cheval, H., Selfridge, J. & Bird, A. The role of MeCP2 in the brain. *Annu. Rev. Cell Dev. Biol.* **27,** 631–652 (2011).
3. Tudor, M., Akbarian, S., Chen, R. Z. & Jaenisch, R. Transcriptional profiling of a mouse model for Rett syndrome reveals subtle transcriptional changes in the brain. *Proc. Natl Acad. Sci. USA* **99,** 15536–15541 (2002).

4. Jordan, C., Li, H. H., Kwan, H. C. & Francke, U. Cerebellar gene expression profiles of mouse models for Rett syndrome reveal novel MeCP2 targets. *BMC Med. Genet.* **8,** 36 (2007).
5. Chahrour, M. *et al.* MeCP2, a key contributor to neurological disease, activates and represses transcription. *Science* **320,** 1224–1229 (2008).
6. Ben-Shachar, S., Chahrour, M., Thaller, C., Shaw, C. A. & Zoghbi, H. Y. Mouse models of MeCP2 disorders share gene expression changes in the cerebellum and hypothalamus. *Hum. Mol. Genet.* **18,** 2431–2442 (2009).
7. Samaco, R. C. *et al. Crh* and *Oprm1* mediate anxiety-related behavior and social approach in a mouse model of MECP2 duplication syndrome. *Nature Genet.* **44,** 206–211 (2012).
8. Baker, S. A. *et al.* An AT-hook domain in MeCP2 determines the clinical course of Rett syndrome and related disorders. *Cell* **152,** 984–996 (2013).
9. Zhao, Y. T., Goffin, D., Johnson, B. S. & Zhou, Z. Loss of MeCP2 function is associated with distinct gene expression changes in the striatum. *Neurobiol. Dis.* **59,** 257–266 (2013).
10. King, I. F. *et al.* Topoisomerases facilitate transcription of long genes linked to autism. *Nature* **501,** 58–62 (2013).
11. Sugino, K. *et al.* Cell-type-specific repression by methyl-CpG-binding protein 2 is biased toward long genes. *J. Neurosci.* **34,** 12877–12883 (2014).
12. Meins, M. *et al.* Submicroscopic duplication in Xq28 causes increased expression of the *MECP2* gene in a boy with severe mental retardation and features of Rett syndrome. *J. Med. Genet.* **42,** e12 (2005).
13. Collins, A. L. *et al.* Mild overexpression of MeCP2 causes a progressive neurological disorder in mice. *Hum. Mol. Genet.* **13,** 2679–2689 (2004).
14. Lyst, M. J. *et al.* Rett syndrome mutations abolish the interaction of MeCP2 with the NCoR/SMRT co-repressor. *Nature Neurosci.* **16,** 898–902 (2013).
15. Li, Y. *et al.* Global transcriptional and translational repression in human-embryonic-stem-cell-derived Rett syndrome neurons. *Cell Stem Cell* **13,** 446–458 (2013).
16. Deng, V. *et al. FXYD1* is an MeCP2 target gene overexpressed in the brains of Rett syndrome patients and *Mecp2*-null mice. *Hum. Mol. Genet.* **16,** 640–650 (2007).
17. Lewis, J. D. *et al.* Purification, sequence, and cellular localization of a novel chromosomal protein that binds to methylated DNA. *Cell* **69,** 905–914 (1992).
18. Mellén, M., Ayata, P., Dewell, S., Kriaucionis, S. & Heintz, N. MeCP2 binds to 5hmC enriched within active genes and accessible chromatin in the nervous system. *Cell* **151,** 1417–1430 (2012).
19. Guo, J. U. *et al.* Distribution, recognition and regulation of non-CpG methylation in the adult mammalian brain. *Nature Neurosci.* **17,** 215–222 (2014).
20. Skene, P. J. *et al.* Neuronal MeCP2 is expressed at near histone-octamer levels and globally alters the chromatin state. *Mol. Cell* **37,** 457–468 (2010).
21. Kriaucionis, S. & Heintz, N. The nuclear DNA base 5-hydroxymethylcytosine is present in Purkinje neurons and the brain. *Science* **324,** 929–930 (2009).
22. Szulwach, K. E. *et al.* 5-hmC-mediated epigenetic dynamics during postnatal neurodevelopment and aging. *Nature Neurosci.* **14,** 1607–1616 (2011).
23. Xie, W. *et al.* Base-resolution analyses of sequence and parent-of-origin dependent DNA methylation in the mouse genome. *Cell* **148,** 816–831 (2012).
24. Lister, R. *et al.* Global epigenomic reconfiguration during mammalian brain development. *Science* **341,** 1237905 (2013).
25. Cohen, S. *et al.* Genome-wide activity-dependent MeCP2 phosphorylation regulates nervous system development and function. *Neuron* **72,** 72–85 (2011).
26. Kaneda, M. *et al.* Essential role for de novo DNA methyltransferase Dnmt3a in paternal and maternal imprinting. *Nature* **429,** 900–903 (2004).
27. Polymenidou, M. *et al.* Long pre-mRNA depletion and RNA missplicing contribute to neuronal vulnerability from loss of TDP-43. *Nature Neurosci.* **14,** 459–468 (2011).
28. Raychaudhuri, S. *et al.* Accurately assessing the risk of schizophrenia conferred by rare copy-number variation affecting genes with brain function. *PLoS Genet.* **6,** e1001097 (2010).
29. Darnell, J. C. *et al.* FMRP stalls ribosomal translocation on mRNAs linked to synaptic function and autism. *Cell* **146,** 247–261 (2011).
30. Yazdani, M. *et al.* Disease modeling using embryonic stem cells: MeCP2 regulates nuclear size and RNA synthesis in neurons. *Stem Cells* **30,** 2128–2139 (2012).

Supplementary Information is available in the online version of the paper.

Acknowledgements We thank E. Griffith and members of the Greenberg laboratory, A. Bird, G. Mandel and members of their laboratories, and M. Coenraads for discussions, M. Goodell for providing the *Dnmt3a* mice, N. Sharma and F. DiBiase for experimental support, and M. Mistry of the HSPH Bioinformatics Core, Harvard School of Public Health for assistance with gene expression analysis. This work was supported by grants from the Rett Syndrome Research Trust and the National Institutes of Health (NIH) (1RO1NS048276) to M.E.G., fellowships from the Damon Runyon Cancer Research Foundation (DRG-2048-10) and the William Randolf Hearst fund to H.W.G., as well as NIH grant T32GM007753, and the HHMI Gilliam fellowship to B.K., H.S. is a HHMI Fellow of the Damon Runyon Cancer Research Foundation (DRG-2194-14).

Author Contributions H.W.G. and B.K. performed or directed all experiments and analysis in the study. H.W.G., B.K. and D.A.H. performed gene expression analysis. B.K. performed EMSA assays. H.W.G. performed ChIP-seq analysis. H.W.G., H.S., N.R.K. performed bisulfite sequencing and DNA methylation analysis. H.W.G., D.A.H., H.S., N.R.K. and M.H. performed bioinformatics and statistical analysis. H.W.G., B.K. and C.S.G. performed Dnmt3a mouse experiments and neuronal culture experiments. D.H.E. provided mouse reagents. H.W.G., B.K. and M.E.G. wrote the manuscript. M.E.G. advised on all aspects of the study.

Author Information Raw data and processed values from RNA-seq, Microarray, ChIP-seq and bisulfite-seq experiments have been submitted to the NCBI Gene Expression Omnibus under accession number GSE60077. Reprints and permissions information is available at www.nature.com/reprints. The authors declare no competing financial interests. Readers are welcome to comment on the online version of the paper. Correspondence and requests for materials should be addressed to M.E.G. (michael_greenberg@hms.harvard.edu).

METHODS

Analysis of published MeCP2-regulated gene lists. To search for unique characteristics of genes found to be misregulated in *Mecp2* mutant mice we interrogated the list of genes found to be significantly activated or repressed by MeCP2 in the cerebellum of MeCP2 KO and MeCP2 OE mice[6]. Using published data sets for the mouse cerebellum from ENCODE and other sources, these genes were assessed for epigenetic marks at promoters and gene bodies, including histone acetylation and methylation as measured by ChIP-seq analysis, as well as DNA methylation and hydroxymethylation as measured by affinity purification methods[18]. In addition, we interrogated sequence attributes of genes, including dinucleotide frequencies, exon number, repeat density within genes and gene length. To determine if the misregulated genes were exceptional with respect to any epigenetic marks or sequence attributes, they were compared to several sets of control genes selected to be matched for gene expression levels (data not shown). Although no obvious epigenetic differences were apparent from this analysis, we detected the extreme length of genes (measured as total basepairs from RefSeq transcription start site to transcription termination site) repressed by MeCP2 (upregulated in the MeCP2 KO and downregulated in the MeCP2 OE). We note that affinity-based measures of DNA methylation that were used in this initial unbiased search are now known to be insensitive to low level methylation at individual cytosines and thus do not report mCA levels with high fidelity. This likely explains why we did not detect a methylation signature for MeCP2-repressed genes using the affinity-based data in our initial analysis. Subsequent analysis of multiple published gene lists from several brain regions revealed the consistent, extreme length of the genes identified as repressed by MeCP2 in each brain region. These findings are presented in Fig. 1a as boxplots where each plot depicts the median (line), the second through to the third quartiles (box), 1.5× the interquartile range (whiskers), and 1.58× the interquartile range/($\sqrt{}$ number of genes) (notches). The notches on each box approximate a 95% confidence interval for the median value[31]. Note that opposing changes in MeCP2 KO and MeCP2 OE published gene lists were used to define genes significantly activated or repressed by MeCP2 for hypothalamus[5], cerebellum[6], and amygdala[7] tissues. For hippocampus[8], striatum[9] and liver[9] MeCP2 KO data alone had been used to identify gene lists.

To test if long gene misregulation is specific to *Mecp2* mutants, we surveyed gene expression studies profiling models of neurological dysfunction, asking if long gene length is a common attribute in gene sets from these studies. We analysed the lengths of the lists of up- and downregulated genes identified in these studies or if 'called' misregulated gene lists were not available, we generated lists using the Genespring 12.6 software package (Agilent Technologies) or the Geo2R analysis tool (http://www.ncbi.nlm.nih.gov/geo/geo2r/). This analysis did not uncover any additional gene sets with similar long length to that of MeCP2 mutant studies (Extended Data Fig. 1a), suggesting that misregulation of extremely long genes is not a common consequence of cell dysfunction in models of neurodegeneration or several other neurological diseases.

To analyse gene expression genome-wide with respect to gene length, CEL files containing the raw hybridization data in from multiple MeCP2 KO and MeCP2 OE gene expression studies were downloaded from GEO (http://www.ncbi.nlm.nih.gov/geo/; study details, sample numbers and genotypes are provided in Supplementary Table 1) and analysed for expression at the gene level using using the GeneSpring software suite (Agilent Technologies) with RMA summarization of 'core' probesets. To facilitate unambiguous analysis of individual genes, expression values for transcript cluster IDs were filtered to include only transcript clusters that map to single RefSeq genes, and expression values for genes with multiple transcript clusters were derived by taking the average $\log_2$ expression value across all transcript clusters corresponding to each gene. To facilitate comparison between microarray platforms, throughout this study we present analysis only for genes represented on all microarray platforms; this corresponds to 14,168 genes for mouse, and 17,989 genes for human. Although this represents a subset of genes in each genome, we have obtained similar results for length-dependent changes in gene expression for expanded gene sets covered by individual platforms (data not shown). In addition, similar results were obtained using the Affymetrix Power Tools pipeline with PLIER as an alternative summarization method. For consistency, microarray data for gene expression in human cells was presented using a comparable array summarization scheme as the mouse microarray data (RMA). Similar qualitative results showing length-dependent gene misregulation were obtained from gene expression values generated by Li and colleagues using a normalization scheme that included spike-controls[15] (summarized transcript expression values were downloaded directly from GEO). However, with this normalization procedure, the absolute values of fold-change of all genes across the entire genome were downshifted in *MECP2* null neurons relative to wild-type. For analysis of RTT patient samples, raw CEL files from Deng *et al.*[16] were downloaded from GEO, and summarized using the RMA function in the R 'affy' package.

To quantify the relationship between fold-change and gene length, we sorted genes by the lengths of their immature transcripts (RefSeq annotation) and employed a sliding window containing 200 consecutive genes in steps of 40 genes. The $\log_2$ fold-change values for the 200 genes within each length bin were averaged and plotted; displayed standard errors for a bin were calculated by propagating the s.e. deduced from the bin's $\log_2$-fold-change values and the mean s.e. of the individual genes reflecting their sample variability. Null distributions displayed on fold-change plots were constructed for each bin from 10,000 random samples of 200 genes selected without regard to transcript length.

RNA sequencing and analysis. Total RNA was prepared from cortex of male wild-type and MeCP2 KO mice at 8–9 weeks of age. Formal power analysis was not used to predetermine sample size, however, sample size (3 per genotype) was determined based on previous detection of length-dependent gene expression effects in data sets that used similar sample sizes (see Fig. 1b, c and Extended Data Fig. 1 and Supplementary Table 1). Animals were preselected based on genotype before collection to ensure that paired samples were taken within litters, but collection was randomized and the experimenter was uninformed of genotype during collection, sample processing, and analysis. Brain samples were dissected on ice in HBSS and immediately frozen in liquid nitrogen. To extract RNA, the tissue was thawed in trizol (Ambion), homogenized, extracted with chloroform, and further purified on RNeasy columns (Qiagen) using on-column DNase treatment to remove residual DNA as specified in the manufacturer's instructions. High-throughput sequencing of total RNA was performed as a service by BGI America. Briefly, ERCC control RNAs (Ambion) were added to samples, and total RNA was depleted of ribosomal RNA using the Ribozero rRNA removal kit (Epicentre), heat-fragmented to 200–700 bp in length and cloned using uracil-N-glycosylase-based strand-specific cloning. cDNA fragments were sequenced using an Illumina HiSeq 2000, typically yielding 20M–40M usable 49 bp single-end reads per sample (Supplementary Table 1 for details). Gene expression levels were assessed using an in-house analysis pipeline previously developed for RNA-seq quantification[32]. After filtering out adaptor and low quality reads, reads were mapped using BWA[33] to the mm9 genome augmented by an additional set of splicing targets (~3M sequences of length ≤ 98 bp representing all possible mm9 sequences that could cross at least one exon-exon junction based on the RefSeq annotation). Samples were normalized based on uniquely mapped reads that fell outside of rRNA and noncoding genes in order to avoid skewing by spikes in incompletely depleted ribosomal and transfer RNA. Normalization of each sample was referred to an in-house standard of 10M 35-bp reads. Gene expression within exons and other features was quantified as 'density', defined as read coverage of that feature, equal to the total number of read bases per total number of feature bases multiplied by the overall normalization coefficient. Units of density are always proportional to RPKM (density = 0.35 × RPKM).

Average read density within a gene's exons was taken as a proxy for gene expression (for genes with multiple annotated transcripts, exonic loci were unioned together). For a given set of samples, a quantile distribution (QD) was constructed from all samples' sorted expression levels, and values from the QD were reassigned to each gene according to its rank in each sample. Within each subset of samples corresponding to wild type (WT), knockout (KO) and so on, each gene was assigned its mean log QD value and a standard error over its values for this subset in order to quantify its sample-to-sample variability within the subset. Precisely zero expression levels were ignored in constructing the QD. The log of the fold-change (FC) between subsets for each gene, for example, log (KO/WT), was set to the difference of the means of the KO and WT log values for the gene, along with a propagated s.e. of the log values (variance equal to the sum of KO and WT variances). For consistency, the RNA-seq analysis in this study is presented for the common set of genes covered by microarray analyses in previous studies (see above). Similar results were obtained for larger sets of genes defined by all RefSeq genes.

To confirm that our findings with RNA-seq were robust to the method of quantification used, we also performed analysis using the spliced transcripts alignment to a reference (STAR)[34] software to align reads to the mm9 genome and Cufflinks[35] to estimate gene-level expression values as fragments per kilobase of exon model per million mapped fragments (FPKM). This analysis yielded results that were nearly identical to those generated using our in-house RNA-seq analysis pipeline. In addition, we derived similar results using transcripts per million (TPM)[36] as the measure mRNA levels in place of FPKM (data not shown).

MeCP2 has previously been implicated in the repression of repeat elements across the mammalian genome, raising the possibility that the upregulation of long genes we observe in our analysis is a reflection of increased transcription from repeat elements or possibly cryptic promoters. To look for changes in the expression of repeat RNAs in the MeCP2 KO brain, RNA-seq reads were mapped to the genome using Bowtie, keeping reads mapping to multiple sites in the genome. Each read was assigned a score of $1/n$ (n = number of sites a read mapped to). Expression values for each repeat family was calculated by adding the scores within each repeat (annotated using Repeatmasker) and normalizing to sequencing depth.

This analysis did not reveal evidence of upregulation of specific repeat classes in the MeCP2 KO brain. In addition, to look for evidence of increased expression of repeats in connection with longer genes we assessed whether there was increased antisense transcription in these genes using our in-house RNA-seq analysis pipeline. This analysis failed to provide evidence of increased antisense transcription. Another alternative explanation for our results was that the increase in expression of long genes we observe is due to spurious transcription, which might initiate from cryptic promoters within genes to generate sense coding, incomplete RNAs. In this case the upregulated RNAs would not reflect mature protein coding mRNA levels. To assess the expression of mature mRNA directly we measured mRNA expression by quantifying only RNA-seq reads that map across exon splice junctions. Consistent with there being an upregulation of mature mRNAs from long genes in the MeCP2 KO, this analysis yielded genome-wide length-dependent upregulation of gene expression that is highly similar to our whole-exon-based approach described above (data not shown). We conclude from this analysis that functional, protein-coding mRNAs derived from long genes are upregulated in the MeCP2 KO, and that this increase is likely due to an alteration in canonical genic transcription mechanisms, not an increase in spurious transcripts coming from long gene loci.

Gene expression analysis of MeCP2(R306C) mice. Consistent with nomenclature from past descriptions of RTT missense mutations, the R306C nomenclature refers to the mouse MeCP2 isoform 2 (MeCP2_e2; NCBI Reference Sequence NP_034918). For gene expression analysis brain regions were dissected from male *Mecp2*^{R306C}/y mice[14] and wild type littermates at 8–10 weeks of age and RNA was isolated as described above. Animals were preselected based on genotype before collection to ensure that paired samples were taken within litters, but collection was randomized and the experimenter was uninformed of genotype during collection, sample processing and analysis. Microarray analysis of cerebellar RNA was performed using the Affymetrix mouse exon 1.0 ST array platform. Analysis was performed in the Dana Farber microarray core facility following manufacturer's recommendations. Analysis of hybridization data was performed as described above. Formal power analysis was not used to predetermine sample size, however sample size (4 per genotype) was determined based on previous detection of length-dependent gene expression effects in data sets that used similar sample sizes (see Extended Data Fig. 1 and Supplementary Table 1).

Validation of microarray and RNA-seq findings. For reverse transcription-quantitative PCR expression analysis candidate genes were selected for analysis in the visual cortex based on consistent upregulation in the MeCP2 KO ($\log_2$-fold-change greater than zero) and downregulation in the MeCP2 OE ($\log_2$-fold-change less than zero) across eight published microarray data sets in five brain regions (hypothalamus, cerebellum, amygdala, striatum, hippocampus). For Nanostring nCounter validation genes were selected based on the above criteria and evidence of upregulation in the visual cortex RNA-seq analysis. Genes with this profile were selected for qPCR assessment in the visual cortex. cDNA was generated from 500 ng of visual cortex total RNA (High-Capacity cDNA Reverse Transcription Kit, Applied Biosystems), and quantitative PCR was performed using transcript-specific primers (designed with the universal probe library design centre, Roche, Supplementary Table 2) and SYBR green detection on the Lightcycler 480 platform (Roche). Relative transcript levels and fold-changes were calculated by normalizing qPCR signal within each sample to six genes that do not show evidence of altered expression across published microarray data sets (Supplementary Table 2). Similar results were obtained by analysing raw Cp values for test transcripts without normalization to control genes (data not shown).

For non-amplification-based gene expression analysis, Nanostring nCounter reporter CodeSets were designed to detect candidate MeCP2-repressed genes in 250 ng of total RNA extracted from MeCP2 KO and MeCP2(R306C) mice. Samples were processed at Nanostring Technologies, following the nCounter Gene Expression protocol. Briefly, total RNA was incubated at 65 °C with reporter and capture probes in hybridization buffer overnight, and captured probes were purified and analysed on the nCounter Digital Analyzer. The number of molecules of a given transcript was determined by normalizing detected transcript counts to the geometric mean of ERCC control RNA sequences and a set of control genes that do not show evidence of altered expression across published microarray data sets. Hotelling T2 test for small sample size[37] was used to calculate significance in order to incorporate variance across both samples and genes. Significant differences between wild-type and MeCP2 KO or MeCP2(R306C) samples ($P < 0.01$) were also detected by paired two-tailed *t*-test comparing the paired mean values for each gene (averaged across samples within each genotype) between genotypes.

Electromobility shift assays. Oligonucleotide probes (Integrated DNA Technologies) were 5′-^{32}P-end-labelled by T4 polynucleotide kinase (New England Biolabs) with [γ-^{32}P]ATP (Perkin Elmer) under conditions recommended by the enzyme supplier. 5′-^{32}P-end-labelled upper strands were purified over NucAway Spin Columns (Ambion) and annealed to equal molar concentration of the appropriate unlabelled complement strand in 10 mM Tris, pH 8.0, 50 mM NaCl, 1 mM EDTA at 95 °C for 5 min, followed by slow cooling to room temperature. Similarly, unlabelled competitors were annealed. Proper annealing of probes and competitors was verified by native gel electrophoresis.

For binding reactions using the MBD fragment of MeCP2, each reaction contained 180 ng of protein (amino acids (AA) 81–170, Abnova or AA 78–162, Diagenode), 50 fmol of 5′-^{32}P-end-labelled probe with an excess of an unlabelled competitor in the presence of 1 μg of poly-dIdC (Sigma), 1× Tris-borate-EDTA (TBE) buffer, 1 mM DTT, 20 mM HEPES, pH 7.5, 0.5 mM EDTA, 0.2% Tween-20, 30 mM KCl, and 1× Orange DNA loading dye (Thermo Scientific). Binding was carried out in a 10 μl volume for 10 min at room temperature. Each reaction was loaded on a 10% non-denaturing polyacrylamide (37.5:1, acrylamide/bis-acrylamide) gel in 1X TBE buffer and electrophoresed for 30 min at 240 V on ice. For binding reactions using the full-length MeCP2 protein, each reaction contained 60 ng of protein (AA 1–486, Millipore), 100 fmol of 5′-^{32}P-end-labelled probe with an excess of unlabelled competitor in the presence of 250 ng of pdIdC (Sigma), 0.5× Tris-borate-EDTA (TBE) buffer, 1 mM DTT, 20 mM HEPES, pH 7.5, 0.5 mM EDTA, 0.2% Tween-20, 30 mM KCl, and 1× Orange DNA loading dye (Thermo Scientific) in a 10 μl reaction volume for 10 min at room temperature. Each reaction was loaded on a 6% non-denaturing polyacrylamide gel (Life Technologies) in 0.5× TBE buffer and electrophoresed for 25 min at 300 V on ice. Gels were then dried on Whatman filter paper on a gel drier at 80 °C for 1 h. For imaging, dried gels were exposed to film overnight (Kodak X-Omat XB film) at −80 °C.

Whole-genome bisulfite sequencing and analysis. For bisulfite sequencing analysis cerebella and cortices from four, eight-week-old mice were dissected and genomic DNA extracted. Starting with 25 ng of genomic DNA, 0.25 ng of unmethylated lambda DNA was added and libraries were generated using the Ovation Ultralow Methyl-Seq Library System (Nugen). Bisulfite treatment was performed using the EpiTect bisulfite conversion kit (Qiagen) following manufacturer's instructions. Libraries were constructed using TruSeq reagents (Illumina) and sequenced on the Hiseq 2000 or Miseq instruments (Illumina). Reads were mapped to the mm9 genome using BS seeker[38], allowing up to four mismatches. Duplicate reads were removed and only uniquely mapping reads were kept (Supplementary Table 1 for details). For analysis of published bisulfite sequencing data sets[19,24], short read files were downloaded from GEO, mapped, and analysed as described above, or processed data files showing number of reads and number of non-converted reads per cytosine base were used (Supplementary Table 1 for details). Methylation levels in all data sets were calculated as number of cytosine base calls/(number of cytosine + number of thymine base calls) within mapped reads at genomic sites where the reference genome encodes cytosine. For hydroxymethylation analysis, the same approach was applied to Tet-assisted bisulfite sequencing (TAB-seq) data from cortical tissue[24]. To examine the effects of gene body methylation independently of promoters, only genes greater than 4.5 kb and with a minimal coverage of CGs and CHs were used in our analysis, and methylation levels within regions of the transcription start site +3 kb to transcription end site were calculated by taking the average methylation levels for all reads mapping within this region. Comparison to gene expression data was performed using corresponding microarray expression values for the hippocampus and the cerebellum or RNA-seq from the cortex. To facilitate fold-change analysis of RNA-seq data, the genes analysed were filtered for minimal (non-zero) expression values.

MeCP2 chromatin immunoprecipitation analysis. MeCP2 ChIP analysis was performed on cortex and cerebella dissected from 8-week-old wild-type male mice as previously described[25,39]. To facilitate direct comparison of MeCP2 ChIP to published frontal cortex DNA methylation and hydroxymethylation data[24], we also performed MeCP2 ChIP analysis using the same brain region at the same developmental stage (frontal cortex isolated from 6-week-old mice). ChIP DNA was cloned into libraries and sequenced on the Illumina HiSeq 2000 or Hiseq 2500 platform to generate 49 or 50 bp single-end reads. Reads were mapped to mouse genome mm9 using BWA[33] and custom perl scripts were employed to quantify read density (reads per kb) for each gene. Normalized read density values were calculated as reads per kb in each genomic feature (for example, gene), normalized to the total number of reads sequenced for each sample, and divided by the reads per kb in that feature for the input DNA that was isolated before the ChIP and sequenced in parallel. As with the methylation analysis, gene bodies were defined as +3,000 bp to the predicted transcription termination site in the RefSeq gene model. To ensure sufficient coverage and accurate assessment of density in gene bodies, only genes greater than 4,500 bp in total length with at least one read in the input sample were included in the analysis.

To explore the relationship between MeCP2 binding and mCA at high resolution, we also quantified the MeCP2 ChIP signal from the frontal cortex in 500-bp bins tiled for all genes in the genome and compared it to mCA levels derived from high-coverage DNA methylation analysis of this brain region (Extended Data Fig. 4)[24]. In addition, we employed the MACS[40] algorithm to identify sites of

MeCP2 ChIP enrichment, or 'summits', across the genome and looked for evidence of mCN at these sites. Due to the broad binding of MeCP2 across the genome, MeCP2 ChIP yields numerous sites of modest local enrichment (~twofold), not isolated, highly-enriched peaks (>tenfold) that are characteristic of transcription factors. Thus, to define MeCP2 summits, we used a low threshold of MeCP2 ChIP over input enrichment (>onefold) and a low stringency *P* value threshold ($P < 0.2$), which yielded 31,479 summits of MeCP2 ChIP signal. Aggregate plots across all 31,479 MeCP2 summits were generated using the *annotatePeaks.pl* program in the Hypergeometric Optimization of Motif EnRichment (HOMER)[41] software. Input-normalized MeCP2 ChIP signal was calculated as the ratio of MeCP2 ChIP/input read coverage. Log_2 enrichment of mCN under MeCP2 summits was determined by calculating the level of methyl-cytosine (number of non-converted cytosines sequenced)/(number of converted and non-converted cytosines sequenced) occurring at CA, CC, CT, or CG positions in the genome, normalized to the flanking region (mean of −4 kb to −3 kb and 3 kb to 4 kb region relative to the MeCP2 summit). The average value for the ChIP signal or relative mCN was then calculated for windows (100-bp for ChIP, 10-bp for mCN) tiled across each summit location and averaged across all of the 31,479 summits of MeCP2 ChIP enrichment identified using the MACS peak-calling algorithm[40] (red) and 31,479 randomly selected control sites (grey).

Analysis of *Dnmt3a*$^{fl/fl}$; *Nestin-Cre*$^{+/-}$ mice. Female *Dnmt3a*$^{fl/fl}$ mice[26] (kindly provided by M. Goodell) were bred to male *Nestin-Cre*$^{+/-}$ mice[42] to generate *Dnmt3a*$^{fl/+}$; *Nestin-Cre*$^{+/-}$ animals. To ensure expression of the imprinted *Nestin-Cre* transgene, male *Dnmt3a*$^{fl/+}$ Tg(Nes-cre)1Kln/J animals were bred to *Dnmt3a*$^{fl/fl}$ females to generate *Dnmt3a*$^{fl/fl}$ Tg(Nes-cre)1Kln/J conditional knockout mice ("Dnmt3a cKO") and *Dnmt3a*$^{fl/fl}$ control animals ('control'). For western blot, DNA methylation and gene expression analyses, cerebella were dissected from 10-11-week-old animals. Proteins were resolved by SDS–PAGE and immunoblotted using the following antibodies: Dnmt3a (abcam, ab13888), MeCP2 (custom antisera[43]) and Gapdh (Sigma Aldrich, #G9545-25UL). Genotyping for the *Dnmt3a* locus was performed by PCR with primers flanking both *loxP* sites (F: 5′-GCAGC AGTCCCAGGTAGAAG-3′, R: 5′-ATTTTTCATCTTACTTCTGTGGCATC-3′) on DNA derived from tails. The presence of the *Cre* allele was detected using primers to this transgene (F: 5′-GCAAGTTGAATAACCGGAAATGGTT-3′, R: 5′-AGGGTGTTATAAGCAATCCCCAGAA-3′). This genotyping scheme allows for simultaneous assessment of the presence of the floxed allele and the relative level of *loxP* recombination that has occurred in the sample. Brain-specific recombination was confirmed by PCR of tail DNA compared to cerebellar DNA (see Extended Data Fig. 7). For gene expression analysis RNA was extracted and analysed as described above for MeCP2(R306C) cerebellum samples.

Identification and analysis of MeCP2-repressed genes. To facilitate identification of genes repressed by MeCP2 in the context of extremely small changes in gene expression, we analysed the 14,168 common genes quantified across eight published microarray 'training data sets' in five brain regions (hypothalamus, cerebellum, amygdala, striatum, hippocampus), applying the lowest possible threshold for fold-change (fold-change >0 in the MeCP2 KO, fold-change <0 in the MeCP2 OE) but demanding consistent misregulation in the predicted direction (at least 7 out of 8 data sets). Genes meeting this minimal threshold for direction of change were then filtered for minimum average change in gene expression (>7.5%), yielding 466 MeCP2-repressed genes (Supplementary Table 3). To determine if there 466 genes represent a significant population of reproducibly affected genes in MeCP2 mutants above what would be expected by chance we performed 7×10^5 resampling iterations, calculating the number of genes meeting the MeCP2-repressed criteria when the gene identity was randomized with respect to the calculated fold-change. This analysis yielded an average of 31 genes per iteration (observed/expected = 466/31 = 15) and did not detect an instance of 466 or more genes meeting the MeCP2-repressed criteria (maxium of 60 genes per iteration), thus yielding a significance of $P < 1.5 \times 10^{-6}$. The robustness of this gene list for predicting misregulation in *Mecp2* mutants is demonstrated by the reproducible upregulation of these genes in the 'test data sets' in Extended Data Fig. 8. Negative control data sets used in this analysis to test for specificity were identified through a survey of available GEO data sets. To qualify for analysis they were required to have a minimum number of biological replicates similar to the MeCP2 data sets (>4) and to have been analysed on either of the microarray platforms used for the training data sets (Affymetrix MoGene 1.0 ST, or MoExon 1.0 ST). For individual gene analysis we calculated the significance of misregulation for individual example genes across the 10 *Mecp2* mutant data sets displayed in Extended Data Fig. 8 as follows: after confirming a normal distribution of fold-change values in each data set, we calculated a *z* score for the fold-change of each gene in each data set. Assuming the null hypothesis that each gene would be randomly sampled from a standard normal distribution, a *t* statistic was derived from the mean and standard error of the gene's *z* scores across the data sets, and this sample's *P* value was calculated from the *t* distribution for nine degrees of freedom. While the analysis presented here utilizes these 466 genes identified on the criteria described above, similar results for gene length, enriched overlap with FMRP target genes, and enrichment for neuronal annotations were obtained with gene lists generated using alternative criteria (for example, up in MeCP2 KO, down in MeCP2 OE in 8 out 8 data sets without minimum expression threshold).

Gene ontology analysis was performed using the DAVID v6.7 bioinformatics resource[44] (http://david.abcc.ncifcrf.gov/), using the 14,168 genes covered in our analysis as background. Overlap of MeCP2-repressed genes with FMRP target genes was performed by mapping putative FMRP target lists[29,45] to the 14,168 genes used for identification of MeCP2-repressed genes. Data processing, plotting, and statistical analysis were performed using available packages and custom scripts in R.

Brain-specific expression of long genes. To assess expression of long genes across neural and non-neural tissues, RNA-seq data sets for seven mouse tissues dissected from eight-week-old mice[46] and ten human tissues[47] were mapped and quantified as described above. Similar results of brain-specific long gene expression were obtained for microarray data from the wild type samples of the five brain regions analysed in *Mecp2* mutant studies compared to the wild type liver (data not shown).

Neuronal cell culture and topotecan treatment. Primary cortical neurons were prepared from E16.5 mouse embryos and cultured as described by Kim *et al.*[33]. For lentiviral-mediated shRNA knockdown, virus was prepared as described in Tiscornia *et al.*[48] using the MeCP2 shRNA and control shRNA plasmids previously validated in Zhou *et al.*[49]. Virus was concentrated and titrated using the GFP signal expressed from IRES GFP in the virus. After one day *in vitro* (DIV), cells were infected with lentivirus (knockdown or control) at an MOI of ~5, such that >90% of cells were infected. On DIV 4 cells were fed (neurobasal media with AraC, 2 μM final concentration) and subsequently treated with various dilutions of topotecan in DMSO (0.05% DMSO final concentration). At DIV 10, cells were collected in trizol for RNA analysis, or protein gel loading buffer for protein. RNA samples were processed and analysed using the Nanostring nCounter assay as described above, with the exception that 6 control genes were used for normalization. Western blot analysis to confirm knockdown of MeCP2 was performed as described in Chen *et al.*[43]. Mean values shown in Extended Data Fig. 9 ($n = 3$–5) are derived from separate cultures obtained from independent litters of mice (independent biological replicates), dissected on separate days, cultured and collected independently.

Regulatory Approval. All animal experiments were performed in accordance with regulations and procedures approved by the Harvard Medical Area Standing Committee on Animals (HMA IACUC).

31. McGill, R., Tukey, J. & Larsen, W. A. Variations of box plots. *Am. Stat.* **32,** 12–16 (1978).
32. Li, H. & Durbin, R. Fast and accurate short read alignment with Burrows–Wheeler transform. *Bioinformatics* **25,** 1754–1760 (2009).
33. Kim, T. K. *et al.* Widespread transcription at neuronal activity-regulated enhancers. *Nature* **465,** 182–187 (2010).
34. Dobin, A. *et al.* STAR: ultrafast universal RNA-seq aligner. *Bioinformatics* **29,** 15–21 (2013).
35. Trapnell, C. *et al.* Differential gene and transcript expression analysis of RNA-seq experiments with TopHat and Cufflinks. *Nature Protocols* **7,** 562–578 (2012).
36. Wagner, G. P., Kin, K. & Lynch, V. J. Measurement of mRNA abundance using RNA-seq data: RPKM measure is inconsistent among samples. *Theory in Biosciences* **131,** 281–285 (2012).
37. Wu, Y., Genton, M. G. & Stefanski, L. A. A multivariate two-sample mean test for small sample size and missing data. *Biometrics* **62,** 877–885 (2006).
38. Chen, P. Y., Cokus, S. J. & Pellegrini, M. B. S. Seeker: precise mapping for bisulfite sequencing. *BMC Bioinformatics* **11,** 203 (2010).
39. Ebert, D. H. *et al.* Activity-dependent phosphorylation of MeCP2 threonine 308 regulates interaction with NCoR. *Nature* **499,** 341–345 (2013).
40. Feng, J., Liu, T. & Zhang, Y. Using MACS to identify peaks from ChIP-seq data. *Current Protocols in Bioinformat.* **Chapter 2**, Unit 2 14 (2011).
41. Nagy, G., Daniel, B., Jonas, D., Nagy, L. & Barta, E. A novel method to predict regulatory regions based on histone mark landscapes in macrophages. *Immunobiology* **218,** 1416–1427 (2013).
42. Tronche, F. *et al.* Disruption of the glucocorticoid receptor gene in the nervous system results in reduced anxiety. *Nature Genet.* **23,** 99–103 (1999).
43. Chen, W. G. *et al.* Derepression of BDNF transcription involves calcium-dependent phosphorylation of MeCP2. *Science* **302,** 885–889 (2003).
44. Huang da. W., Sherman, B. T. & Lempicki, R. A. Systematic and integrative analysis of large gene lists using DAVID bioinformatics resources. *Nature Protocols* **4,** 44–57 (2009).
45. Brown, V. *et al.* Microarray identification of FMRP-associated brain mRNAs and altered mRNA translational profiles in fragile X syndrome. *Cell* **107,** 477–487 (2001).
46. Mortazavi, A., Williams, B. A., McCue, K., Schaeffer, L. & Wold, B. Mapping and quantifying mammalian transcriptomes by RNA-seq. *Nature Methods* **5,** 621–628 (2008).
47. Gray, J. M. *et al.* SnapShot-Seq: a method for extracting genome-wide, *in vivo* mRNA dynamics from a single total RNA sample. *PLoS ONE* **9,** e89673 (2014).

48. Tiscornia, G., Singer, O. & Verma, I. M. Production and purification of lentiviral vectors. *Nature Protocols* **1,** 241–245 (2006).
49. Zhou, Z. *et al.* Brain-specific phosphorylation of MeCP2 regulates activity-dependent Bdnf transcription, dendritic growth, and spine maturation. *Neuron* **52,** 255–269 (2006).
50. Valinluck, V. *et al.* Oxidative damage to methyl-CpG sequences inhibits the binding of the methyl-CpG binding domain (MBD) of methyl-CpG binding protein 2 (MeCP2). *Nucleic Acids Res.* **32,** 4100–4108 (2004).
51. Hashimoto, H. *et al.* Recognition and potential mechanisms for replication and erasure of cytosine hydroxymethylation. *Nucleic Acids Res.* **40,** 4841–4849 (2012).
52. Spruijt, C. G. *et al.* Dynamic readers for 5-(hydroxy)methylcytosine and its oxidized derivatives. *Cell* **152,** 1146–1159 (2013).
53. Khrapunov, S. *et al.* Unusual characteristics of the DNA binding domain of epigenetic regulatory protein MeCP2 determine its binding specificity. *Biochemistry* **53,** 3379–3391 (2014).

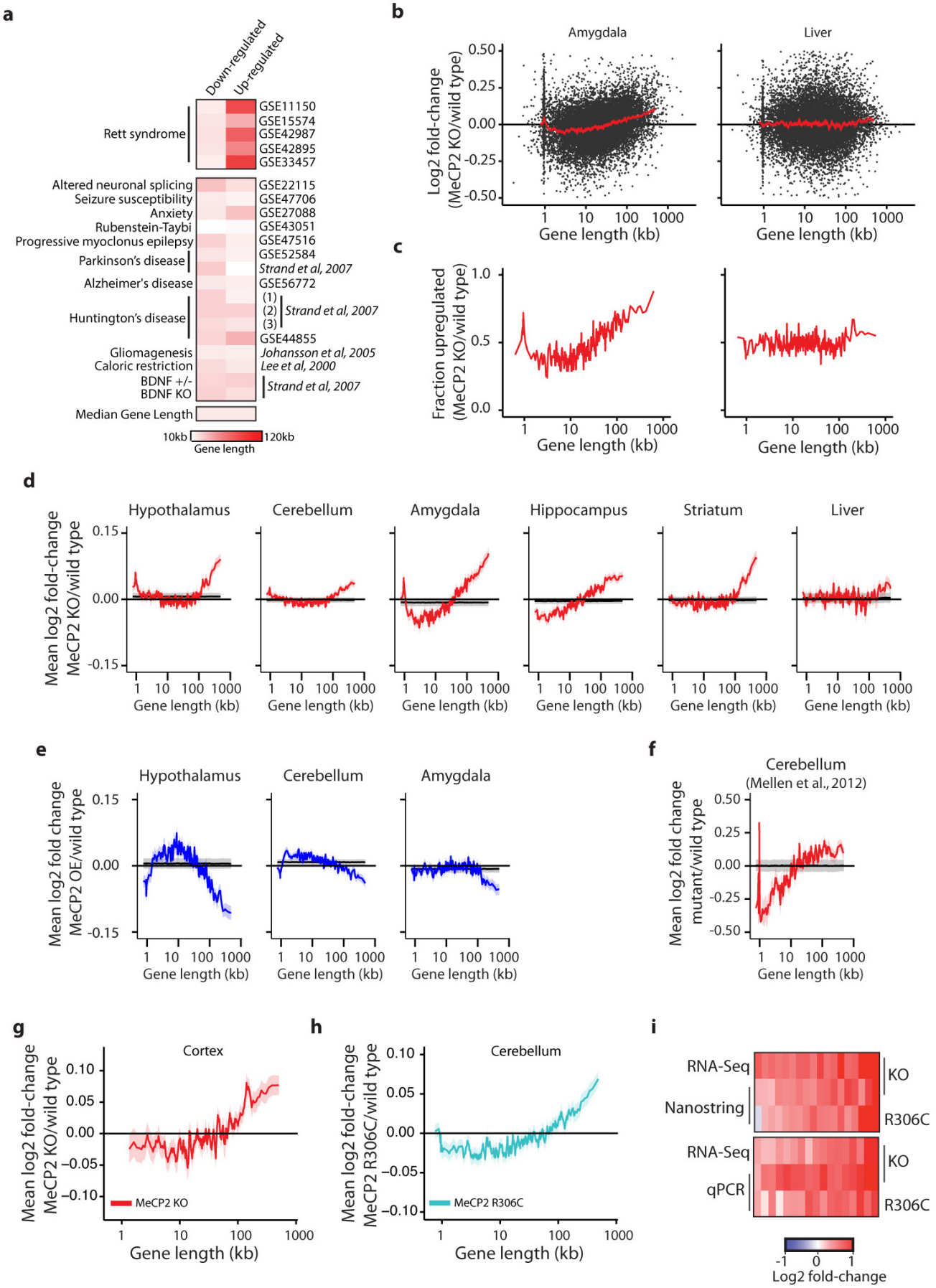

Extended Data Figure 1 | Analysis of gene expression changes in *Mecp2* mutant mice. **a**, Heatmap of median gene lengths for genes identified as misregulated in *Mecp2* mutant studies or sixteen different studies of neurological dysfunction and disease in mice. Mouse model and GEO accession number, or reference, are listed (for Strand *et al.* (1), 3NP treatment; (2), human HD brain; (3), R2/6 *Htt* transgenic). **b**, Scatter plots of fold-change in gene expression in the MeCP2 KO for the amygdala (left), which shows robust length-dependent misregulation, and the liver (right), which does not. Fold-change values for genes (black points) and mean fold-change for 200 genes per bin with a 40 gene step are shown (mean, red line; ribbon, s.e.m.). **c**, The fraction of genes showing fold-change >0 for data sets in **b**; genes binned by length (100 gene bins, 50 gene step). **d**–**f**, Analysis of published microarray[5–9] (**d**, **e**) or RNA sequencing (RNA-seq)[18] (**f**) data sets from MeCP2 KO (**d**, **f**) or OE (**e**) mice. Mean fold-change in expression (200 gene bins, 40 gene step), red line; ribbon, s.e.m. For **d**–**f**, mean (black line) and two standard deviations (grey ribbon) are shown for 10,000 resamplings in which gene lengths were randomized with respect to fold-change. The spike in mean fold-change at ~1 kb in several plots corresponds to the olfactory receptor genes (Supplementary Discussion). **g**, Mean changes in expression of genes binned by length from RNA-seq analysis of MeCP2 KO cortex ($n = 3$ per genotype). **h**, Mean changes in expression from microarray analysis of genes binned by length in MeCP2(R306C) cerebellum ($n = 4$ per genotype) **i**, Heatmap summary of fold-changes in gene expression from RNA-seq analysis of *Mecp2* mutant mean in **g** compared to Nanostring nCounter (18 genes, top) or RT-qPCR (17 genes, bottom) analysis from cortex ($n = 4$ per genotype). Selected long genes (>100 kb) consistently upregulated in the MeCP2 KO or downregulated in MeCP2 OE mutant mice across brain tissues were tested (Supplementary Table 2). A statistically significant upregulation of these genes is observed in the cortex for both MeCP2 KO (nCounter, $P = 0.00073$; qPCR, $P < 1 \times 10^{-15}$) and MeCP2(R306C) (nCounter, $P = 0.0482$; qPCR, $P = 1.69 \times 10^{-6}$; Hotelling T^2 test for small sample size[37]). Note that for completeness, data from other figures have been re-presented here. See Methods and Supplementary Table 1 for sample sizes from published data sets and other details.

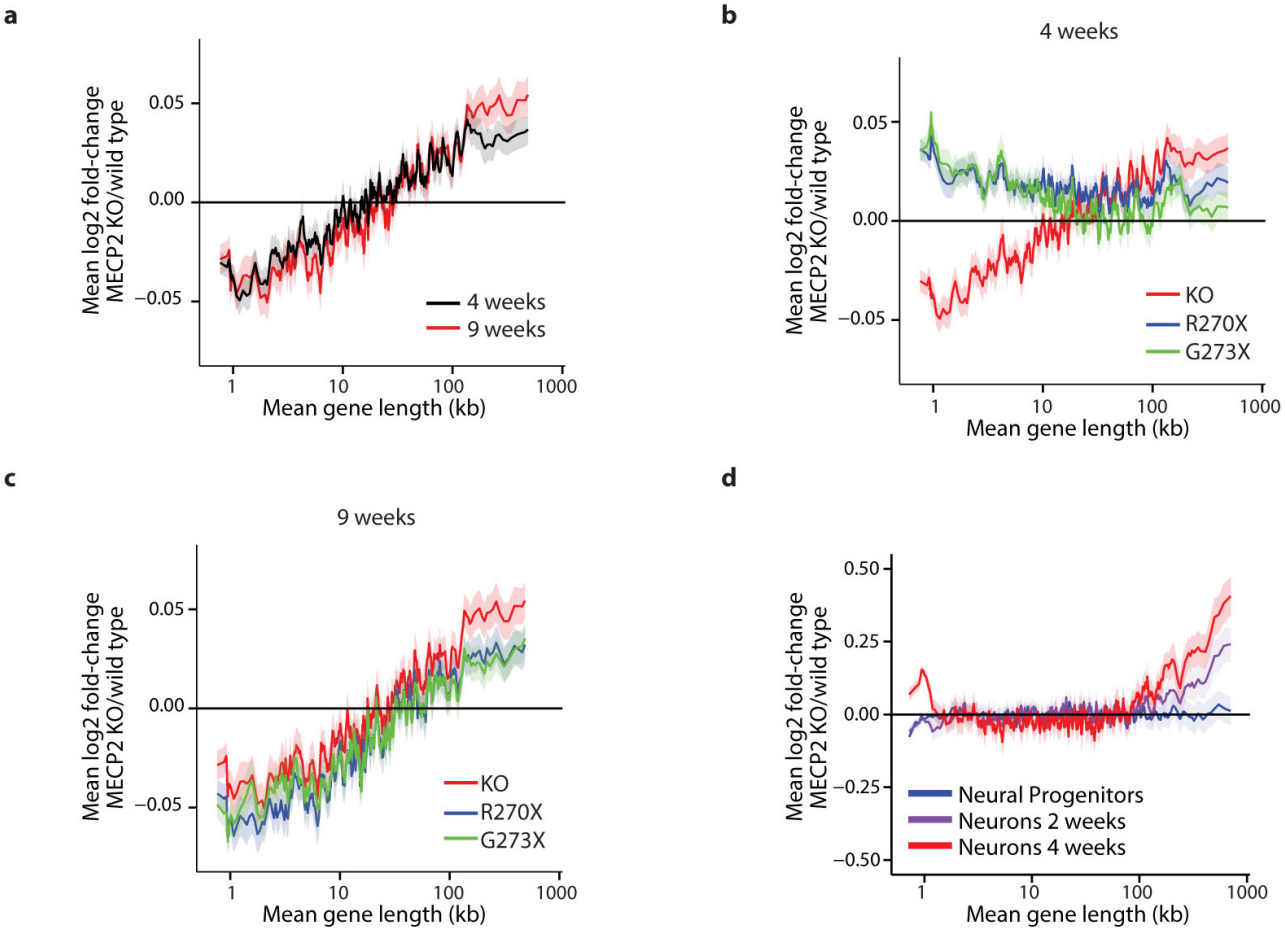

Extended Data Figure 2 | Timing and severity of gene expression changes in models of RTT. **a**, Mean fold-change in gene expression versus gene length in the hippocampus of MeCP2 KO mice compared to wild type at four and nine weeks of age reveals increasing magnitude of length-dependent gene misregulation that parallels the onset of RTT-like symptoms in these animals[8]. **b**, Mean fold-change in gene expression versus gene length in hippocampus of mice expressing truncated forms of MeCP2 mimicking human disease-causing alleles at four weeks of age. Re-expression of a longer truncated form of MeCP2(G273X) in the MeCP2 KO normalizes expression of long genes more effectively than expression of a shorter truncation of MeCP2(R270X), and parallels the higher degree of phenotypic rescue observed in MeCP2(G273X)-expressing mice compared to MeCP2(R270X)-expressing mice[8]. **c**, Mean fold-change in gene expression versus gene length in hippocampus of mice expressing truncated MeCP2 at nine weeks of age. Consistent with the eventual onset of symptoms of these mouse strains, length-dependent gene misregulation is evident in both strains. **d**, Changes in gene expression for genes binned by length in human *MECP2* null ES cells differentiated into neural progenitor cells, neurons cultured for 2 weeks, or neurons cultured for 4 weeks[15]. In all plots, lines represent mean fold-change in expression for each bin (200 gene bins, 40 gene step), and the ribbon is s.e.m. of genes within each bin. See Methods and Supplementary Table 1 for all sample sizes and other details.

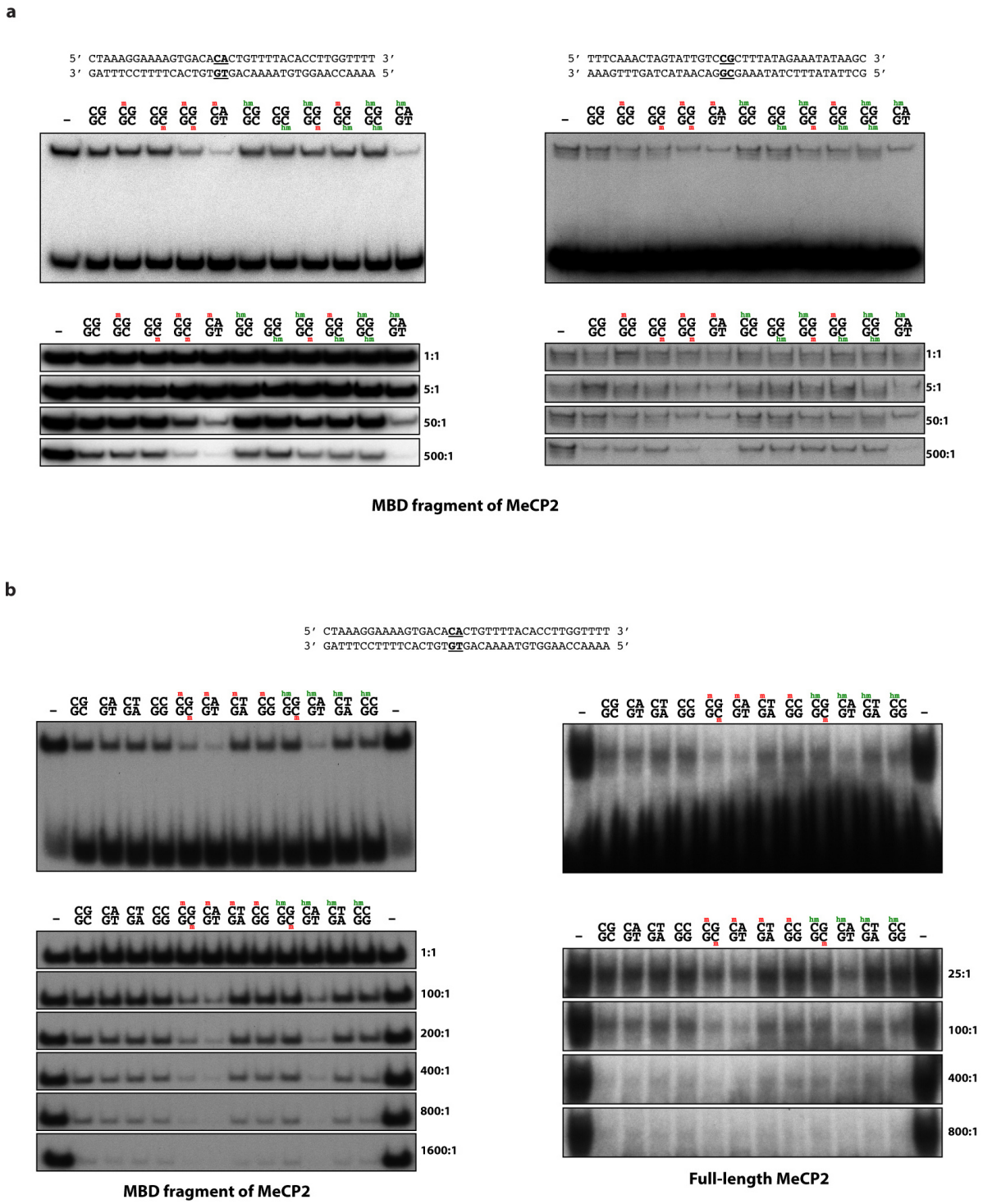

Extended Data Figure 3 | High affinity of MeCP2 for mCG, mCA and hmCA in electrophoretic mobility shift assays. a, Binding of the recombinant methyl-binding domain (MBD) of MeCP2 (amino acids 81–170) to ^{32}P-end-labelled oligonucleotides containing a methylated cytosine in a CA (left) or a CG (right) context competed with unlabelled competitor substituted with unmethylated, methylated, or hydroxymethylated cytosine in a CG or CA context (indicated in bold). Representative full gels showing shifted and unshifted probe in the presence of 50-fold excess of unlabelled competitor (top); close-up of shifted bands over a range of unlabelled competitor (bottom). A mCA-containing oligonucleotide competes for MeCP2 binding with equal or higher efficacy to that of a symmetrically methylated CG oligonucleotide. While hmCG-containing probes compete with similar efficacy to an unmethylated probe, a hmCA-containing probe competes with high efficacy. This difference in affinity of MeCP2 for hmCA- and hmCG-containing probes may explain conflicting results reported for the affinity of MeCP2 for hydroxymethylated DNA[18,50–53](Supplementary Discussion). **b**, Binding and competition of recombinant MeCP2 MBD (amino acids 78–162, left) or full-length MeCP2 (amino acids 1–486, right) incubated with ^{32}P-end-labelled oligonucleotides containing a methylated cytosine in a CA context and competed with oligonucleotides containing unmethylated, methylated, or hydroxymethylated cytosine in a CG, CA, CT, or CC context. Representative full gels showing 100-fold excess of unlabelled competitor (top); close-up of shifted bands over a range of unlabelled competitor (bottom). The results obtained from competitors containing mCG, mCA, hmCG and hmCA are similar to those shown in **a**. In addition, both (h)mCT- and (h)mCC-containing oligonucleotides compete for MeCP2 binding with similar efficacy to that of an unmethylated probe. All results shown were observed in at least two independent experiments.

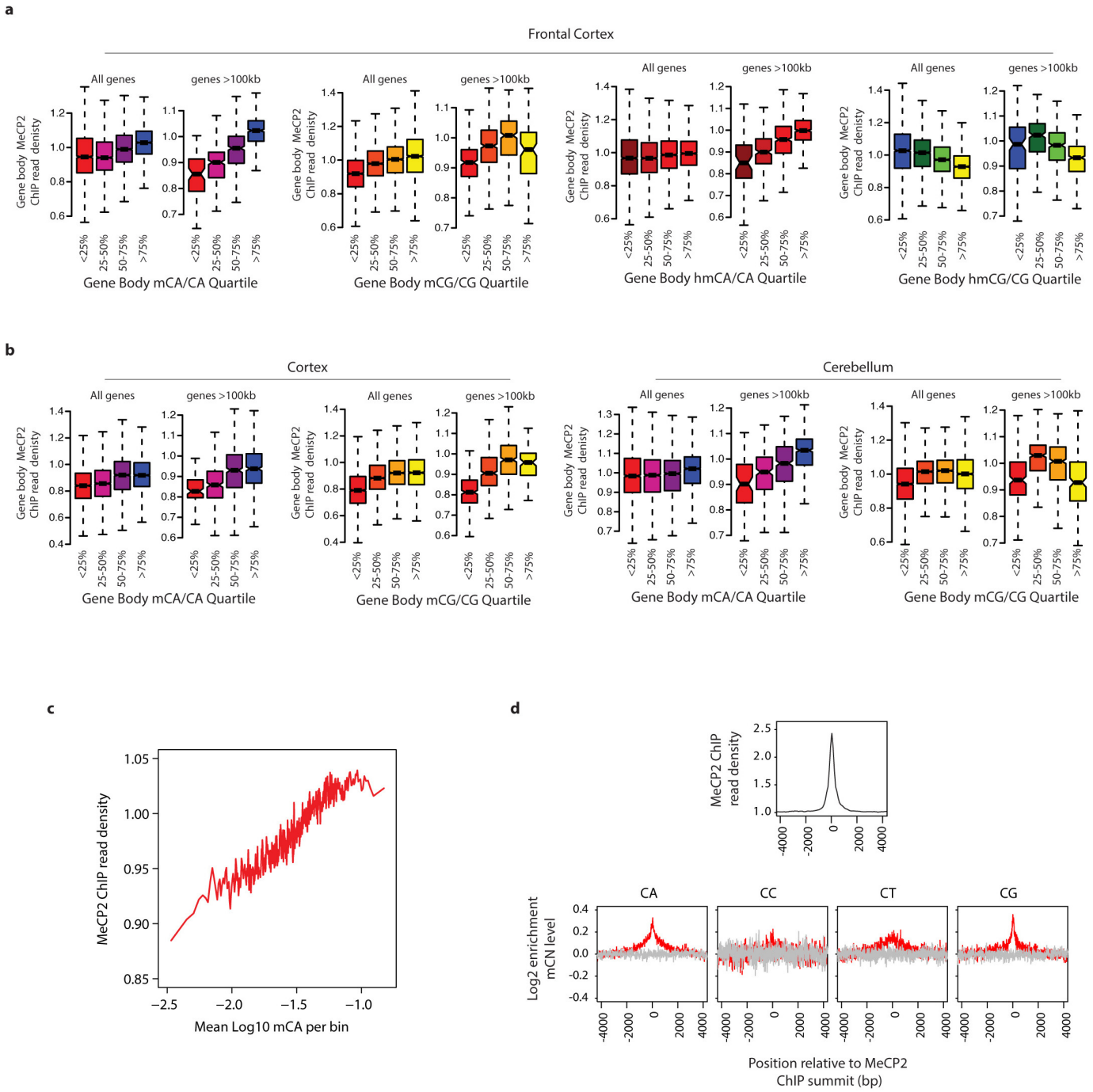

Extended Data Figure 4 | ChIP-seq analysis of MeCP2 binding *in vivo*. **a**, Boxplots of input-normalized read density within gene bodies (TSS +3 kb to TTS) for MeCP2 ChIP from the mouse frontal cortex plotted for genes according to quartile of mCA/CA, mCG/CG, hmCA/CA and hmCG/CG in the frontal cortex[24] for all genes and genes >100 kb. **b**, Similar analysis of MeCP2 ChIP from the mouse cortex (left) or cerebellum (right) plotted for genes according to quartile of mCA/CA or mCG/CG for all genes and genes > 100 kb. MeCP2 ChIP-signal is correlated with mCA/CA levels from the frontal cortex, cortex, and cerebellum for all genes and this correlation is more prominent among genes >100 kb. mCG does not show as prominent a correlation with MeCP2 ChIP signal, and hmCG trends towards anti-correlation with MeCP2 ChIP. These results suggest that MeCP2 has a lower affinity for hmCG than mCG, suggesting that, *in vivo*, hmCG is associated with reduced MeCP2 occupancy (Supplementary Discussion). **c**, High resolution analysis of high-coverage bisulfite sequencing data from the frontal cortex showing a correlation between MeCP2 ChIP signal and mCA. Input-normalized ChIP signal plotted for mCA levels for 500-bp bins tiled across all genes. **d**, Aggregate plots of MeCP2 input-normalized ChIP signal (top) and relative methylation (log_2 enrichment in mC as compared to the flanking regions) for mCA, mCC, mCT, and mCG (bottom) are plotted around the 31,479 summits of MeCP2 ChIP enrichment identified using the MACS peak-calling algorithm[40] (red) or 31,479 randomly selected control sites (grey, see Methods). See Methods and Supplementary Table 1 for sample sizes and other details.

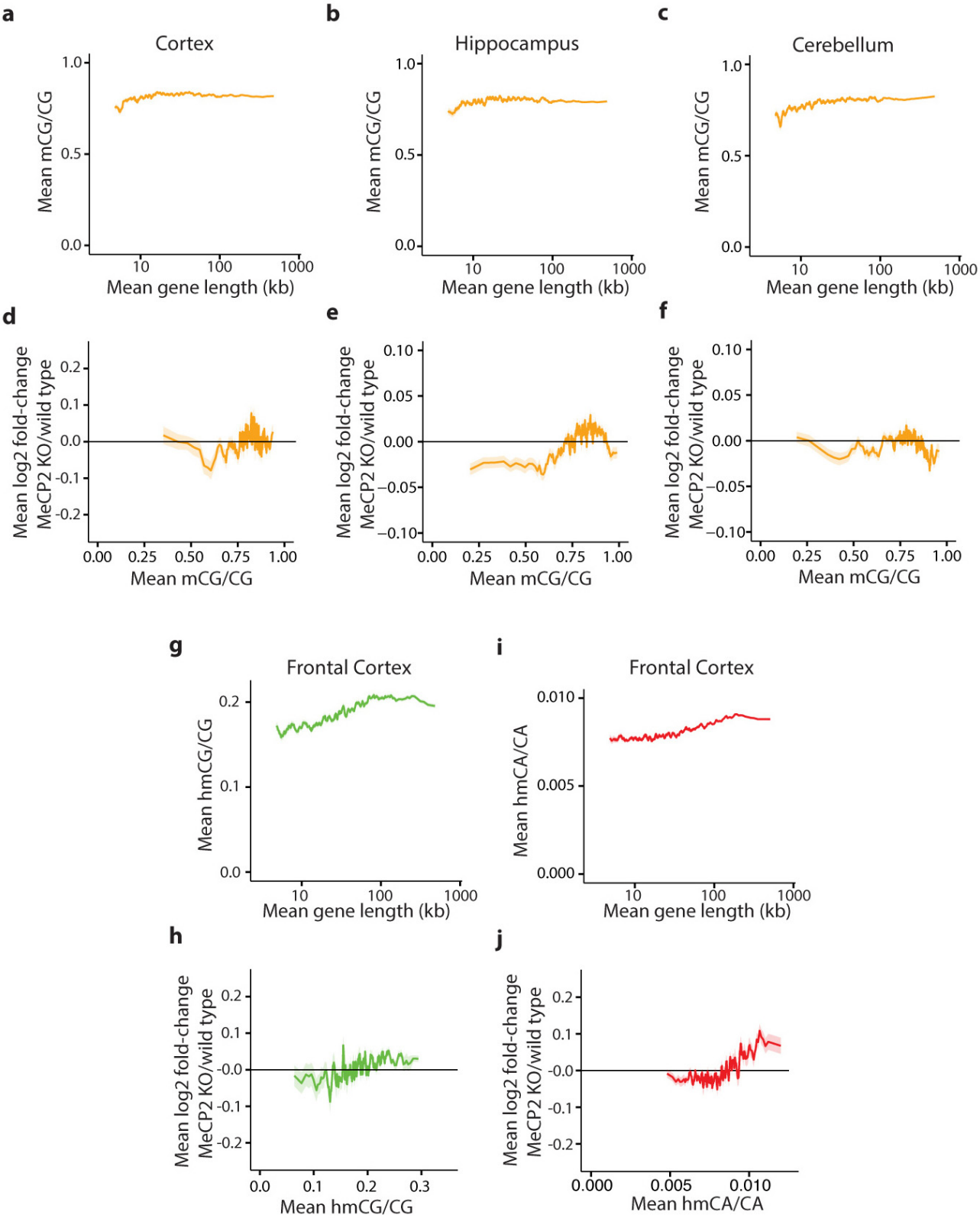

Extended Data Figure 5 | Genomic analysis of mCG, hmCG, and hmCA in length-dependent gene regulation by MeCP2. **a**–**c**, Mean methylation of CG dinucleotides (mCG/CG) within gene bodies (transcription start site +3 kb, up to transcription termination site) in the cortex (**a**), hippocampus (**b**) and cerebellum (**c**) for genes binned according to length. **d**–**f**, Mean fold-change in gene expression in MeCP2 KO compared to wild type in the cortex (**d**), hippocampus (**e**), and cerebellum (**f**) for genes binned according to mCG levels (mCG/CG) within gene bodies. **g**, Mean hmCG levels (hmCG/CG) within gene bodies in the frontal cortex[24] for genes binned according to length. **h**, Mean fold-change in gene expression in MeCP2 KO compared to wild type for genes binned according to hmCG levels (hmCG/CG) within gene bodies in the frontal cortex[24] **i**, Mean hmCA levels (hmCA/CA) within gene bodies in the frontal cortex[24] for genes binned according to length. **j**, Mean fold-change in gene expression in MeCP2 KO compared to wild type genes binned according to hmCA levels (hmCA/CA) within gene bodies in the frontal cortex[24]. In all panels, mean values for each bin are indicated as a line (200 gene bins, 40 gene step); ribbon depicts s.e.m. for genes within each bin. See Methods and Supplementary Table 1 for sample sizes and other details.

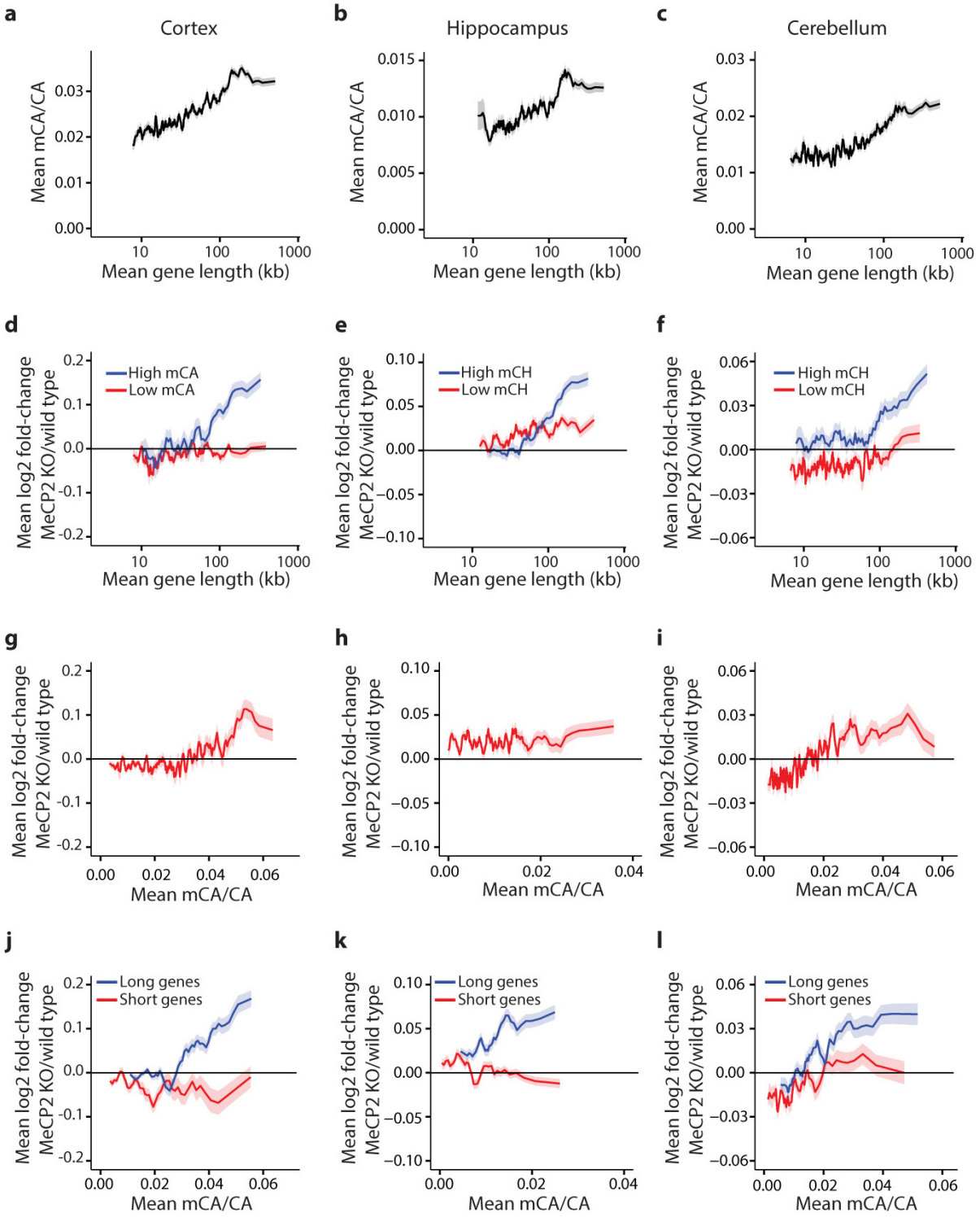

Extended Data Figure 6 | Genomic analysis supports a role for mCA in length-dependent gene regulation by MeCP2. **a**–**c**, Mean methylation at CA dinucleotides (mCA/CA) within gene bodies (TSS +3 kb to TTS) in cortex (**a**), hippocampus (**b**), and cerebellum (**c**) for genes binned by length. **d**–**f**, Mean changes in gene expression in cortex (**d**), hippocampus (**e**), and cerebellum (**f**) of MeCP2 KO for high mCA genes (top 25% mean gene body mCA/CA) and low mCA genes (bottom 66% mean gene body mCA/CA) binned by length. **g**–**i**, Mean changes in gene expression in cortex (**g**), hippocampus (**h**), and cerebellum (**i**) of MeCP2 KO for genes binned according to average gene body mCA/CA levels. **j**–**l**, Mean changes in gene expression in cortex (**j**), hippocampus (**k**), and cerebellum (**l**) of MeCP2 KO mice for long genes (top 25%) and short genes (bottom 25%) in each brain region binned by gene body mCA/CA level. A correlation between fold-change in the MeCP2 KO and mCA/CA for all genes is less prominent, or not observed, in the hippocampus and cerebellum for all genes together (**h**, **i**), but it is clear for the longest genes in the genome analysed alone (**k**, **l**). Note that average levels of mCA appear lower in hippocampus and cerebellum compared to cortex (compare *y* axis in **a**, **b** and **c**), and may explain why a correlation across all genes in not detected in these brain regions. In long genes analysed alone the cumulative effect of higher mCA levels and integration across the gene may be larger, resulting in a detectable effect. In all panels, the line indicates the mean for 200 gene bins, with a 40 gene step; ribbon depicts s.e.m. for genes within each bin. Note that, for completeness, data from analysis of the cortex presented in Fig. 2 are re-presented here. See Methods and Supplementary Table 1 for sample sizes and other details.

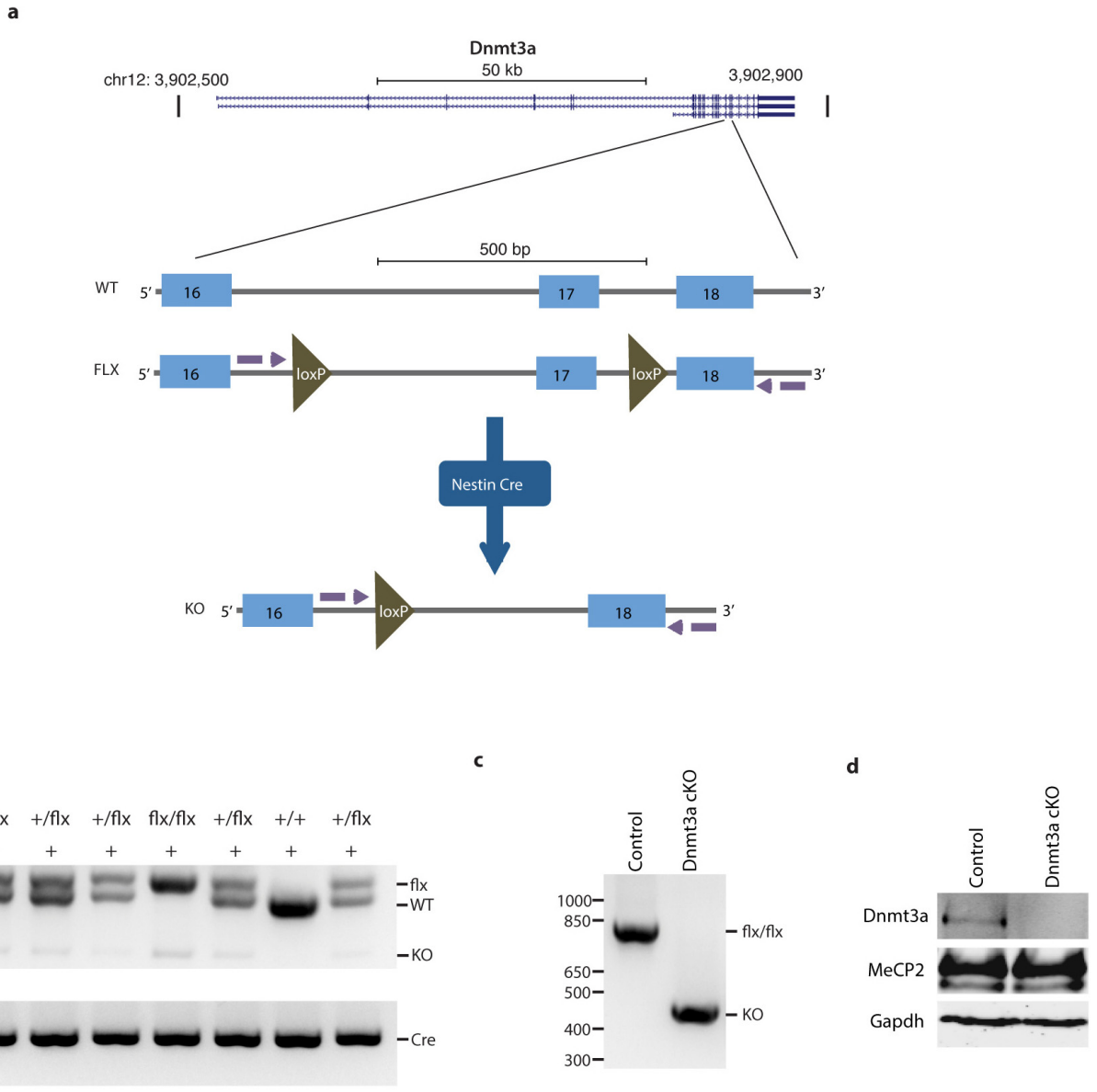

Extended Data Figure 7 | Conditional knockout of Dnmt3a *in vivo*. **a**, Diagram of the *Dnmt3a* locus and Cre-dependent conditional knockout strategy for *Dnmt3a*[26]. *LoxP* sites (green triangles) flank exon 17, which is removed following Cre-mediated recombination. Primers (purple arrows) were designed to flank exons 17 and 18. The wild-type (WT), floxed (FLX), and knockout (KO) allele are depicted. **b**, Representative PCR genotyping for tail DNA samples indicates presence or absence of the floxed (flx, ~800 bp), wild-type (WT, ~750 bp), and knockout (KO, ~500 bp) alleles. Separate genotyping reaction for the *Nestin-cre* transgene (~250 bp) is shown. **c**, Efficient excision of the floxed exon is detected in cerebellar DNA from conditional knockout (*Dnmt3a*$^{flx/flx}$; *Nestin-Cre*$^{+/-}$, Dnmt3a cKO) mice but not from and control animals (*Dnmt3a*$^{flx/flx}$, Control). **d**, Western blot analysis of Dnmt3a, MeCP2, and Gapdh (loading control) protein from the cerebellum of control and Dnmt3a cKO adult mice. All results shown were observed in at least two independent experiments.

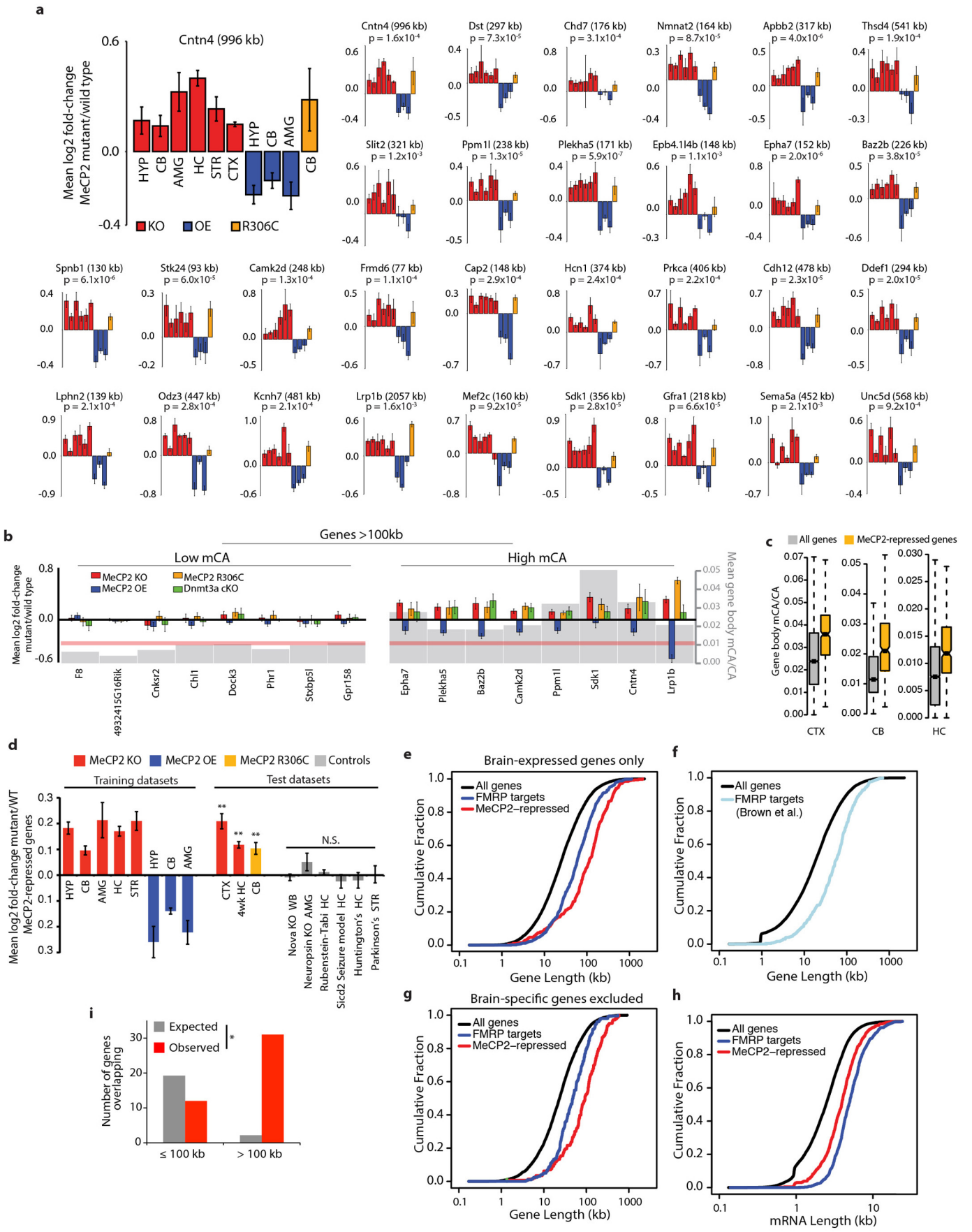

Extended Data Figure 8 | Analysis of MeCP2-repressed genes and FMRP target genes. **a**, Mean fold-change in mRNA expression for examples of MeCP2-repressed genes across three different *Mecp2* mutant genotypes (KO, OE, and R306C) and six brain regions. *P* values for each gene are derived from the mean *z* scores for fold-change across all data sets (see Methods). **b**, Gene expression and CA methylation data from the cerebellum for selected MeCP2-repressed genes from **a** (right), as well as examples of extremely long genes (>100 kb) that are not enriched for mCA and are not misregulated (left). Fold-changes in mRNA expression in *Mecp2* mutants and the *Dnmt3a* cKO are shown (left axis), as well as mean mCA levels (grey; right axis). Red line indicates genomic median for gene body mCA/CA **c**, Boxplots of mCA levels in MeCP2-repressed genes compared to all genes. **d**, Mean fold-change for MeCP2-repressed genes in eight 'training data sets' used to define these genes (see Methods), and nine 'test data sets': three *Mecp2* mutant data sets not used to define MeCP2-repressed genes (CTX MeCP2 KO and CB MeCP2(R306C), generated in this study; HC MeCP2 KO 4 week, analysed from Baker *et al.*[8]), and six data sets from brains of mouse models of neurological dysfunction generated using the same microarray platforms as the MeCP2 data sets (GEO accession numbers in order: GSE22115, GSE27088, GSE43051, GSE47706, GSE44855, GSE52584). Error bars are s.e.m. of MeCP2–repressed gene expression across samples ($n = 4$–8 microarrays per genotype per data set); $^{**}P < 0.01$, one-tailed *t*-test, Benjamini–Hochberg correction. Note that significance testing was not performed on training data sets. Brain regions indicated as in Fig. 1, (WB, whole brain). **e**, Cumulative distribution function (CDF) of gene lengths plotted exclusively for genes that are among the top 60% of expression levels in the brain (Supplementary Discussion). The extreme length of MeCP2-repressed genes and genes encoding FMRP target mRNAs[29] when controlling for expression level indicates that the long length of these genesets is not a secondary effect of the preferential expression of long genes in the brain ($P < 1 \times 10^{-15}$ for each geneset versus all expressed genes; two-sample Kolmogorov–Smirnov test). **f**, The CDF of gene lengths for all genes compared to an independent set of FMRP targets identified by Brown and colleagues[45] ($P < 1 \times 10^{-15}$, Kolmogorov–Smirnov-test). **g**, CDF of gene lengths for genes expressed at similar levels in the brain and other somatic tissues (Supplementary Discussion). The extreme length of each geneset ($P < 1 \times 10^{-15}$, Kolmogorov–Smirnov test) when filtering for genes that are expressed in all tissues indicates that regulation of long genes by MeCP2 and FMRP is not dependent on brain-specific expression. **h**, CDF of mature mRNA lengths for MeCP2-repressed genes, and FMRP target genes ($P < 1 \times 10^{-11}$ for each geneset versus all genes, Kolmogorov–Smirnov test). **i**, Overlap of MeCP2-repressed genes and putative FMRP target mRNAs[29] ($P < 5 \times 10^{-5}$, hypergeometric test). Expected overlap was calculated by dividing the expected overlap genome-wide (hypergeometric distribution) according to the distribution of all gene lengths in the genome. See Methods and Supplementary Table 1 for sample sizes and other details.

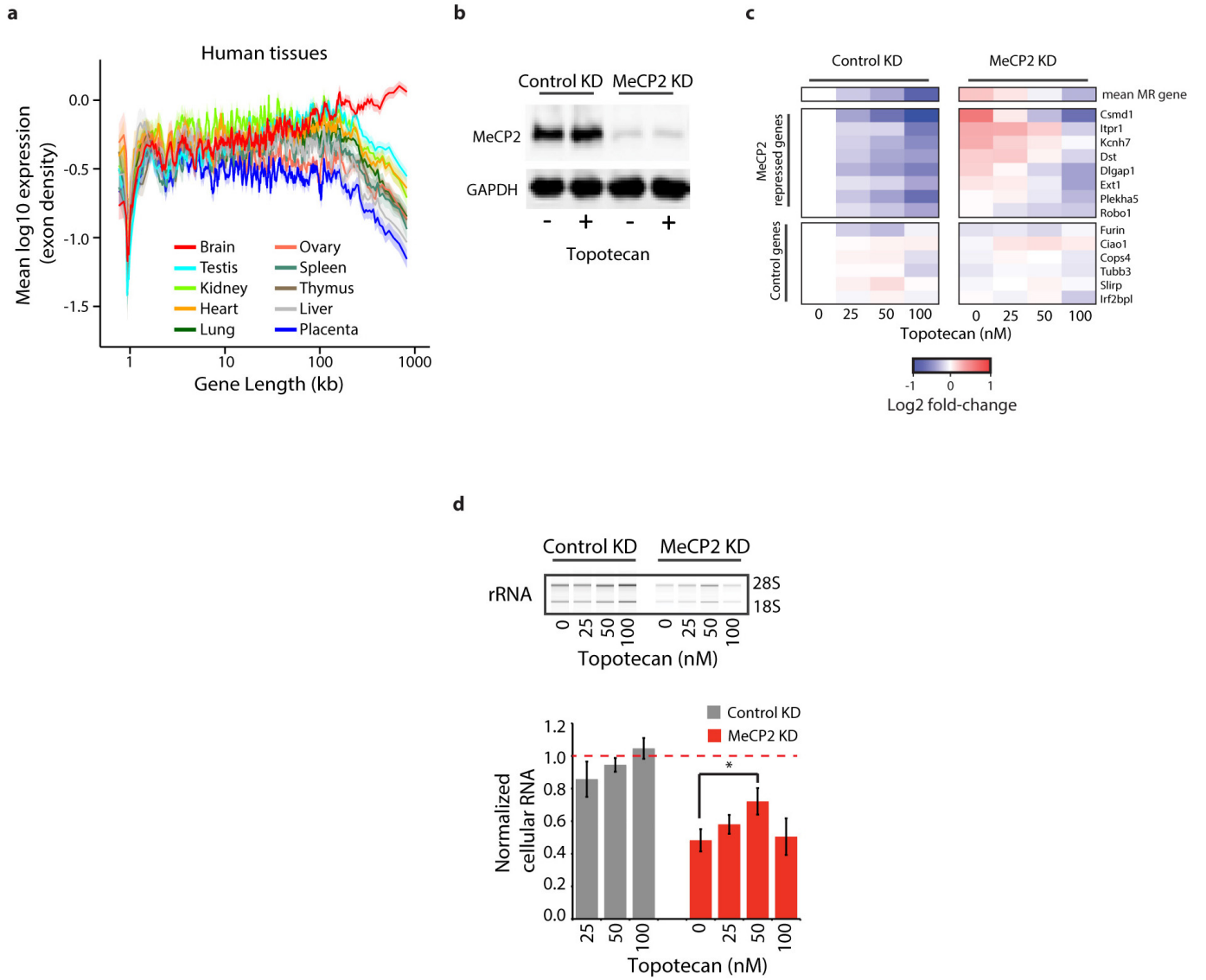

Extended Data Figure 9 | Consequences of long gene misregulation in neurons. **a**, Mean expression of genes binned according to length in human neural and non-neural tissues. Mean expression for genes within each bin (200 gene bins, 40 gene step) is indicated by the line; ribbon represents the s.e.m. of genes within each bin. **b**, Western blot analysis of MeCP2 from primary cortical neurons after control or MeCP2 shRNA knockdown (KD) and treatment with DMSO vehicle (−) or topotecan (+). **c**, Heatmap summary of nCounter analysis for the expression of selected MeCP2-repressed (MR) genes from primary neurons treated with control or MeCP2 shRNA and topotecan ($n = 3$–4). Normalized $\log_2$ fold-change relative to the DMSO-treated, control KD is shown. MeCP2 KD conditions are significantly different from control, ($P = 1 \times 10^{-4}$, repeated measures ANOVA across 8 genes). Newman–Keuls corrected, post-hoc comparisons: $P < 0.05$ control KD, 0 nM drug versus MeCP2 KD, 0 nM drug; $P > 0.05$, control KD, 0 nM drug versus MeCP2 KD, 50 nM drug; $P < 0.05$ MeCP2 KD, 0 nM drug versus MeCP2 KD, 50 nM drug. **d**, Bioanalyzer profiles of 18S and 28S ribosomal RNA (top) and total RNA quantification (bottom) for treated neurons ($n = 3$–5). Total RNA values normalized to DMSO-treated control KD, red dashed line. Two-way repeated measures ANOVA indicates a significant effect of KD ($P < 0.01$) and drug treatment ($P < 0.05$). Rescue assessed by one-tailed t-test, Bonferroni multiple testing correction, $^*P < 0.05$.

Extended Data Table 1 | Gene ontology analysis of MeCP2-repressed genes and genes >100 kb

MeCP2 Repressed Genes (466 genes)

GO Term	Gene Count	EASE pval	Fold Enriched	Benjamini pval	GO Accession
Biological Process					
axon guidance	17	3.7E-08	5.6	6.3E-05	GO:0007411
axonogenesis	21	6.5E-08	4.3	5.5E-05	GO:0007409
cell morphogenesis involved in differentiation	23	2.4E-07	3.7	1.4E-04	GO:0000904
neuron projection morphogenesis	21	2.6E-07	4	1.1E-04	GO:0048812
cell morphogenesis involved in neuron differentiation	21	3.6E-07	3.9	1.2E-04	GO:0048667
neuron projection development	23	3.9E-07	3.6	1.1E-04	GO:0031175
neuron development	26	9.3E-07	3.1	2.3E-04	GO:0048666
cell projection morphogenesis	21	1.3E-06	3.6	2.8E-04	GO:0048858
cell morphogenesis	26	2.1E-06	3	4.0E-04	GO:0000902
cell part morphogenesis	21	3.3E-06	3.4	5.5E-04	GO:0032990
phosphate metabolic process	49	3.3E-06	2	5.1E-04	GO:0006796
phosphorus metabolic process	49	3.3E-06	2	5.1E-04	GO:0006793
cellular component morphogenesis	27	4.2E-06	2.8	5.9E-04	GO:0032989
cell projection organization	26	5.2E-06	2.8	6.8E-04	GO:0030030
enzyme linked receptor protein signaling pathway	24	8.5E-06	2.9	1.0E-03	GO:0007167
Cellular Component					
plasma membrane	110	2.00E-05	1.4	5.3E-03	GO:0005886
cell junction	29	4.30E-05	2.3	5.7E-03	GO:0030054
cytoskeleton	50	6.00E-05	1.8	5.4E-03	GO:0005856
postsynaptic density	8	2.40E-04	6.2	1.6E-02	GO:0014069
synapse	21	3.80E-04	2.4	2.0E-02	GO:0045202
plasma membrane part	64	8.20E-04	1.5	3.6E-02	GO:0044459
cell fraction	29	2.10E-03	1.8	7.9E-02	GO:0000267
basement membrane	8	2.60E-03	4.2	8.3E-02	GO:0005604
neuron projection	16	3.10E-03	2.4	8.7E-02	GO:0043005
synapse part	14	3.20E-03	2.6	8.3E-02	GO:0044456
insoluble fraction	26	3.50E-03	1.9	8.3E-02	GO:0005626
membrane fraction	25	4.50E-03	1.8	9.7E-02	GO:0005624
postsynaptic membrane	10	4.90E-03	3.1	9.7E-02	GO:0045211
Molecular Function					
cation binding	148	5.00E-07	1.4	2.6E-04	GO:0043169
metal ion binding	147	5.50E-07	1.4	1.4E-04	GO:0046872
ion binding	149	7.50E-07	1.4	1.3E-04	GO:0043167
calcium ion binding	47	8.50E-06	2	1.1E-03	GO:0005509
actin binding	21	2.00E-04	2.6	2.1E-02	GO:0003779
cytoskeletal protein binding	26	3.80E-04	2.2	3.3E-02	GO:0008092
protein kinase activity	33	5.30E-04	1.9	3.9E-02	GO:0004672
cation channel activity	18	8.40E-04	2.5	5.3E-02	GO:0005261
voltage-gated cation channel activity	12	1.10E-03	3.2	6.3E-02	GO:0022843
alkali metal ion binding	16	1.40E-03	2.6	6.8E-02	GO:0031420
metal ion transmembrane transporter activity	19	1.90E-03	2.3	8.6E-02	GO:0046873
voltage-gated ion channel activity	14	1.90E-03	2.7	7.9E-02	GO:0005244
voltage-gated channel activity	14	1.90E-03	2.7	7.9E-02	GO:0022832
potassium ion binding	11	2.20E-03	3.2	8.6E-02	GO:0030955

Genes Longer that 100KB (1431 genes)

GO Term	Gene Count	EASE pval	Fold Enriched	Benjamini pval	GO Accession
Biological Process					
phosphate metabolic process	150	1.2E-18	2	3.4E-15	GO:0006796
phosphorus metabolic process	150	1.2E-18	2	3.4E-15	GO:0006793
protein modification process	191	8.3E-18	1.8	1.2E-14	GO:0006464
protein amino acid phosphorylation	120	4.1E-17	2.2	4.0E-14	GO:0006468
biopolymer modification	191	1.4E-15	1.7	1.0E-12	GO:0043412
phosphorylation	124	2.7E-15	2	1.6E-12	GO:0016310
cellular component organization	247	1.1E-14	1.6	5.5E-12	GO:0016043
biological adhesion	101	2.4E-14	2.2	1.0E-11	GO:0022610
cell adhesion	101	2.4E-14	2.2	1.0E-11	GO:0007155
post-translational protein modification	156	1.4E-13	1.8	5.0E-11	GO:0043687
cellular process	849	1.6E-13	1.1	5.2E-11	GO:0009987
nervous system development	137	4.9E-13	1.8	1.4E-10	GO:0007399
cell projection organization	65	9.0E-11	2.3	2.4E-08	GO:0030030
cell morphogenesis	62	2.3E-10	2.3	5.6E-08	GO:0000902
neuron development	59	8.2E-10	2.3	1.8E-07	GO:0048666
Cellular Component					
synapse	74	7.9E-17	2.8	4.4E-14	GO:0045202
cell junction	86	2.5E-13	2.3	5.0E-11	GO:0030054
neuron projection	58	3.4E-13	2.8	4.5E-11	GO:0043005
cell projection	96	1.4E-12	2.1	1.4E-10	GO:0042995
cytoskeleton	149	2.9E-12	1.7	2.3E-10	GO:0005856
plasma membrane	325	5.3E-12	1.4	3.5E-10	GO:0005886
plasma membrane part	205	5.5E-12	1.6	3.1E-10	GO:0044459
extracellular matrix part	30	2.5E-11	4	1.2E-09	GO:0044420
basement membrane	24	1.8E-09	4.1	8.0E-08	GO:0005604
synapse part	43	1.1E-08	2.6	4.2E-07	GO:0044456
proteinaceous extracellular matrix	56	1.4E-08	2.2	4.9E-07	GO:0005578
axon	31	1.8E-08	3.1	6.1E-07	GO:0030424
extracellular matrix	57	2.3E-08	2.2	7.1E-07	GO:0031012
dendrite	29	4.8E-08	3.1	1.4E-06	GO:0030425
postsynaptic membrane	29	2.2E-07	2.9	5.8E-06	GO:0045211
Molecular Function					
calcium ion binding	138	1.4E-15	2	1.2E-12	GO:0005509
protein kinase activity	111	1.6E-15	2.2	6.6E-13	GO:0004672
adenyl ribonucleotide binding	209	9.3E-15	1.7	2.6E-12	GO:0032559
cytoskeletal protein binding	85	1.5E-14	2.4	3.1E-12	GO:0008092
GTPase regulator activity	72	1.2E-13	2.5	2.0E-11	GO:0030695
nucleoside binding	215	1.5E-13	1.6	2.1E-11	GO:0001882
adenyl nucleotide binding	212	2.6E-13	1.6	3.1E-11	GO:0030554
purine nucleoside binding	213	2.8E-13	1.6	2.9E-11	GO:0001883
ATP binding	202	3.0E-13	1.6	2.8E-11	GO:0005524
nucleoside-triphosphatase regulator activity	72	3.9E-13	2.5	3.3E-11	GO:0060589
ion binding	412	9.8E-12	1.3	7.5E-10	GO:0043167
metal ion binding	403	2.0E-11	1.3	1.4E-09	GO:0046872
purine ribonucleotide binding	229	2.5E-11	1.5	1.6E-09	GO:0032555
ribonucleotide binding	229	2.5E-11	1.5	1.6E-09	GO:0032553
cation binding	404	3.8E-11	1.3	2.3E-09	GO:0043169

Functional annotation clustering analysis of genes identified as MeCP2-repressed and the longest genes in the genome (>100 kb) was performed using the DAVID bioinformatics resource (DAVID v6.7)[44]. The top fifteen enriched gene ontology terms with $P < 0.01$ (Benjamini multiple testing correction) are listed for ''Biological Process'', ''Cellular Component'', and ''Molecular Function'', respectively.